

The origin of D'' reflections: a systematic study of seismic array data sets

Laura Cobden* and Christine Thomas

Institute für Geophysik, University of Münster, Corrensstraße 24, 48149 Münster, Germany. E-mail: l.j.cobden@uu.nl

Accepted 2013 April 12. Received 2013 April 11; in original form 2012 October 09

SUMMARY

Regional seismic studies of the Earth's deep mantle indicate the presence of *P*- and *S*-wave reflectors at the top of the D'' layer. Such reflectors appear to be laterally intermittent, occur at a range of depths, and produce waveforms whose amplitude and polarity differ at different locations. A number of possible explanations for D'' reflections have been proposed, including: a phase change from perovskite to post-perovskite; thermal or thermochemical discontinuities generated by subducted slabs; alignment of anisotropic minerals and global or small-scale chemical heterogeneity arising perhaps from core–mantle interactions or primitive material. However, some of the observed heterogeneity in D'' structure may be related to lack of consistency between the style, quality and number of seismic observations in different regions, as well as complexity in wave propagation due to 3-D structure. In this study, we present a compilation of observations of D'' reflections for regions in which (1) a reflector is seen in both *P*- and *S*-wave arrivals and (2) consistent array seismology techniques have been applied to infer the properties of the reflectors. Using a recent Monte Carlo thermodynamic modelling method to convert changes in chemistry and mineralogy into changes in seismic velocity, we compare the fit of different isotropic thermochemical structures to the observed seismic properties of D'' reflections, namely the polarity and amplitude of the waveforms. Our results indicate that it may be possible to discriminate between different possible origins for D'' reflections on the basis of polarity observations alone. Amplitude measurements may provide further constraints but must be treated with caution due to a large number of factors, which can influence waveform amplitudes. In regions such as the Caribbean, which are characterized by high-amplitude, negative polarity *P* waveforms and positive polarity *S* waveforms, a phase change from perovskite to post-perovskite provides the most likely explanation for the discontinuity. However, in other regions, notably Siberia and the central Pacific, *P*- and *S* waveforms both display a positive polarity, and multiple explanations for the discontinuity are possible, including subduction-related chemical heterogeneity and anisotropy.

Key words: Mantle processes; Composition of the mantle; Phase transitions; Body waves.

1 INTRODUCTION

During the last 30 years, numerous regional-scale seismic studies have found evidence for abrupt changes in seismic wave speed in the bottom few hundred kilometres of the Earth's mantle (e.g. Lay & Helmberger 1983; Weber & Kornig 1990; Weber 1993; Kendall & Nangini 1996; Wysession *et al.* 1998; Reasoner & Revenaugh 1999; Russell *et al.* 2001; Lay *et al.* 2004; Thomas *et al.* 2004a,b; Wallace & Thomas 2005; Kito *et al.* 2007; Chaloner *et al.* 2009). These seismic discontinuities are usually detected as *PdP* or *SdS* arrivals (Fig. 1), which have a traveltimes and slowness intermediate between

the direct *P* (or *S*) wave, and the *PcP* (or *ScS*) reflection off the core, and can most easily be seen at distances between $\sim 65^\circ$ and 80° . It is widely assumed that *PdP* and *SdS* arrivals are generated by reflection off (and refraction below) structures which demarcate the top of the Earth's D'' layer [the seismically complex boundary layer up to several hundred kilometres thick at the base of the mantle (Bullen 1949)], and for this reason, the reflecting structures are referred to as 'the D'' discontinuity'. However, there is no requirement for the D'' discontinuity to be globally ubiquitous, since in some locations, it is demonstrably absent in the seismic data (e.g. Weber 1993; Kendall & Nangini 1996; Chambers & Woodhouse 2006). Furthermore, the observed traveltimes and amplitudes of *PdP* and *SdS* arrivals vary laterally both within and between different studies, on length scales of tens to thousands of kilometres (e.g. Wysession *et al.* 1998), suggesting both regional- and local-scale lateral variations in the

*Now at: Department of Earth Sciences, Utrecht University, 3581CD Utrecht, The Netherlands.

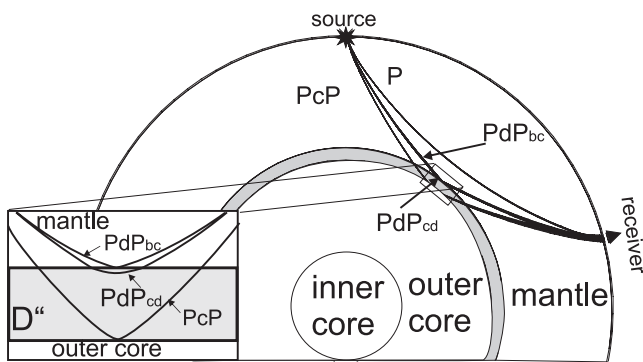


Figure 1. Schematic representation of generation of the PdP phase due to D'' structure above the CMB. P refracts through the mantle; PcP reflects off the CMB, and PdP is a composite phase of a reflection off the top of the D'' discontinuity (PdP_{bc}) and a refraction immediately beneath the discontinuity (PdP_{cd} , sometimes also referred to as PDP). PdP has an arrival time and slowness intermediate between the P and PcP phases. Similar behaviour occurs for S , ScS and SdS phases.

depth, magnitude and sharpness of the discontinuity. On average, the discontinuity is situated ~ 260 km above the core–mantle boundary (CMB), but may vary between 100 and 450 km above the CMB, while estimates of the thickness of the discontinuity range from as little as 8 km to as much as 100 km (e.g. Weber 1993; Wysession *et al.* 1998; Lay 2008). A review of more than 40 data sets by Wysession *et al.* (1998) found that there is no significant correlation between observations of P -wave discontinuities and observations of S -wave discontinuities, and their inferred depth and magnitude probably do not correlate with each other or with long-wavelength (tomographically inferred) seismic structure.

The variability of PdP and SdS observations presents a challenge in deciphering their physical origin. One the one hand, 3-D wave-propagation effects, and modelling trade-offs between the depth, magnitude, topography and sharpness (thickness) of the discontinuity (Liu *et al.* 1998; Wysession *et al.* 1998), make it difficult to place unique constraints on the position and morphology of the discontinuity in a given location (e.g. Kito *et al.* 2007). Added to this, direct comparison between different studies is limited because different data-processing methods and selection criteria are applied in each study. On the other hand, the apparent heterogeneity in D'' discontinuity structure leaves the door open for a plethora of mineralogical, thermochemical and structural explanations for its existence.

Currently, the most popular explanation for the D'' discontinuity is a phase change in $(\text{Mg}, \text{Fe})\text{SiO}_3$ perovskite, the most abundant lower mantle mineral. This possibility was first suggested by Stixrude & Bukowinski (1992). Although no such transformation had been observed experimentally at the time, the idea of a phase change was supported by combined dynamic and seismic modelling by Sidorin *et al.* (1999a,b). According to Sidorin *et al.* (1999b), if the phase change had a positive Clapeyron slope, then lateral variations in the arrival time of PdP and SdS phases could be explained by lateral variations in temperature, which would generate depth variations in the phase transition, while variations in the amplitude of the phases could arise from the superposition of a sharp discontinuity (due to the phase change) onto the local velocity structure. This hypothesis gained credence following the experimental discovery in 2004 of the mineral post-perovskite (Murakami *et al.* 2004; Oganov & Ono 2004; Shim *et al.* 2004), to which perovskite transforms at pressures close to the CMB. The seismic properties of the phase transition in pure MgSiO_3 , namely, a positive Clapeyron slope (Oganov & Ono 2004; Tsuchiya *et al.* 2004) and an increase

in shear velocity of 1–4 per cent in the direction perovskite to post-perovskite accompanied by a smaller increase (<0.5 per cent) in P -wave velocity (Wookey *et al.* 2005; Wentzcovitch *et al.* 2006; Hirose 2007; Stackhouse & Brodholt 2007) are particularly compatible with seismic observations of the D'' discontinuity, which is most frequently modelled as a sharp increase in S -wave velocity of 2–3 per cent and smaller increase in P -wave velocity (e.g. Wysession *et al.* 1998). Consequently, measurements of discontinuity depth and estimated Clapeyron slope have been used to infer lateral and vertical variations in temperature near the CMB (Lay *et al.* 2006; van der Hilst *et al.* 2007), and observations of double or multiple seismic discontinuities within D'' have been interpreted as repeated crossings of the perovskite \leftrightarrow post-perovskite phase boundary (e.g. Hermlund *et al.* 2005; Lay *et al.* 2006; van der Hilst *et al.* 2007; Hutko *et al.* 2008; Kawai & Geller 2010).

However, the lower mantle is (most probably) not composed of pure MgSiO_3 , and once other chemical components are included, the precise depth at which we might expect a perovskite to post-perovskite phase transition inside the Earth, if at all, and the thickness of the transition region, become highly uncertain. This is mainly due to widely varying experimental and theoretical measurements of the effects of Al (Akber-Knutson & Bukowinski 2004; Caracas & Cohen 2005; Oganov & Ono 2005; Tateno *et al.* 2005; Zhang & Oganov 2006; Tsuchiya & Tsuchiya 2008) and Fe (Mao *et al.* 2004; Shieh *et al.* 2006; Tateno *et al.* 2007; Hirose *et al.* 2008). In the presence of Fe-perovskite, Al-perovskite and $(\text{Mg}, \text{Fe})\text{O}$ magnesiowustite, changes in the depth of the phase boundary of up to tens of GPa have been predicted, both above and below the CMB. For a pyrolytic composition—often assumed to represent the ‘average’ mantle chemistry—some experiments indicate that the two-phase transition region containing both perovskite and post-perovskite may have a thickness of up to several hundred kilometres (Catalli *et al.* 2009; Andrault *et al.* 2010), and thus be too broad to generate the D'' discontinuity, although in other experiments, the phase boundary remains relatively sharp (<100 km; Ohta *et al.* 2008). Even if the phase transition in pyrolite is broad, the average lower mantle composition may not be pyrolytic (e.g. Cammarano *et al.* 2005; Cobden *et al.* 2009; Murakami *et al.* 2012), and harzburgitic and basaltic compositions (i.e. subducted materials) may yet be associated with a sharper phase transition, capable of generating a seismic discontinuity (Grocholski *et al.* 2012). Despite the lack of consensus between different studies, it is clear that chemical heterogeneity has the capacity to modify the depth and sharpness of the phase boundary significantly, and thus lateral variability in the amplitude and timing of PdP and SdS phases could reflect lateral variations in both chemistry and temperature at D'' , in the presence of post-perovskite.

Alternatively, sharp seismic discontinuities may be generated by post-perovskite, even when the phase boundary is broad, via anisotropy. Rheological studies on analogue minerals (Hunt *et al.* 2009), as well as first-principles calculations with MgSiO_3 (Amann *et al.* 2010), indicate that a rapid weakening of post-perovskite during the phase transition may produce an abrupt change in anisotropy and therewith a sharp (~ 4 per cent) increase in shear wave velocity if the weak material is deformed by flow.

While post-perovskite has been given much attention recently, other causes for the PdP and SdS arrivals should not be disregarded. Furthermore, PdP and SdS phases need not represent a global (if undulating) discontinuity, but could arise from scattering (Scherbaum *et al.* 1997) off geographically restricted, thermochemically distinct blobs, piles or laminae. Candidate materials include primordial stratification (discussed in Wysession *et al.* 1998); accumulated

subducted material (Christensen 1989; Christensen & Hofmann 1994); or core–mantle reaction products (Knittle & Jeanloz 1989).

In a study of two different regions, Thomas *et al.* (2011) demonstrated that measurements of the waveform amplitudes and polarities of PdP and SdS phases may be used to discriminate between different causes for their origin. The study focused specifically on anisotropy in post-perovskite. While their results indicate that the seismic observations can be explained by anisotropy (via a phase change from perovskite to post-perovskite in which 12 per cent of the anisotropic post-perovskite becomes aligned), anisotropy may not be a unique explanation for the observations. In light of the large experimental uncertainty on the perovskite to post-perovskite phase boundary, together with the expected thermochemical complexity at the base of the mantle due to its convective evolution, we consider here the possibility that PdP and SdS phases could arise not only from a phase change in isotropic perovskite, but also from changes in temperature and (isotropic) mineralogy associated with subduction, mixing and segregation.

We have assembled a collection of measurements of the polarities and amplitudes of PdP and SdS phases from five locations around the world. These measurements have been derived using the same data-processing method, with consistent standards for the detection threshold of the phases, and can thus be directly compared with each other. For each location we extract the polarity and inferred range of amplitudes of the PdP and SdS phases, and assess how well this average seismic structure can be generated by various thermochemical structures. In order to compare seismic observations with physical structures, we use the thermodynamic database

of Stixrude & Lithgow-Bertelloni (2011) to compute seismic velocities for a given mineral assemblage, and a Monte Carlo sampling of the composition space to estimate uncertainties on those velocities (Deschamps *et al.* 2012). We refer to our observations simply as ‘D’ reflections’ because we do not wish to imply a particular length scale for the structures generating those reflections.

To our knowledge, this is the first study which attempts to model the seismic properties of D' reflections statistically, considering the full uncertainties in the mineral physics parameter space, as well as the trade-offs between temperature and composition in generating a particular seismic structure. By performing a robust, fully quantitative interpretation of the seismic data, we hope to provide new insights or constraints on the cause of D' reflections.

2 SEISMIC DATA

PdP and SdS phases are usually too weak to be observed directly on single seismogram traces, and inevitably some kind of stacking technique is required to enhance their visibility. In this study, we use the Vespa stacking process (Davies *et al.* 1971) applied to small seismic arrays, as described in Rost & Thomas (2002, 2009). Small seismic arrays allow us to detect structures in and around D' with a spatial resolution of a few hundred kilometres and lateral extent of up to a few thousand kilometres (Weber 1993). Due to the limited number of installed arrays to date, observation of D' reflections using array methods is currently restricted to a few heterogeneously distributed, geographically narrow patches of the Earth. Nonetheless, compiling observations from different arrays across the world

Table 1. Summary of seismic properties of PdP and SdS phases observed at the locations plotted in Fig. 2.

Region	PdP polarity	Inferred ΔV_p	SdS polarity	Inferred ΔV_s	Array/ Network	Source region	Source–receiver distance (degrees)	References
Siberia	+	1 to 3 per cent	+	2 to 3 per cent	GRSN/GRF	Kuriles/Japan/Hindu Kush	~65–80	^a
Pacific	+	1 to 3 per cent	+	2 to 3 per cent	Polaris CI	Tonga	~70–80	This study
Bering Sea	+	1 to 1.5 per cent	+	1 to 2 per cent	Polaris NWT, BC	West Pacific	~60–85	This study
Caribbean	-	-2 to -3 per cent	+	2 to 3 per cent	California	South America	~65–80	^b
Southeast Asia	-	-1 to -2 per cent	+	1 to 3 per cent	KNET/GHENGIS	Banda Sea	~60–70	^c

Note: Observations are taken from the following studies:

^aThomas *et al.* (2004b, 2011).

^bThomas *et al.* (2004a) and Kito *et al.* (2007).

^cChaloner *et al.* (2009).

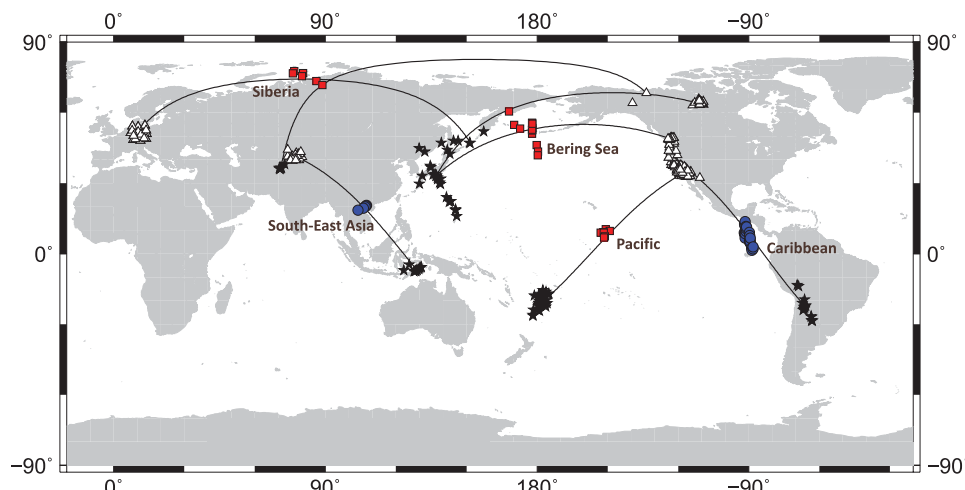


Figure 2. Map showing approximate locations of reflection points of PdP and SdS waves, for the five regions used in this study. Red squares are used for data showing a positive polarity PdP and blue circles for data showing a negative polarity PdP. Locations of events are represented by black stars and stations are indicated by white triangles.

allows us to begin to think about their interpretation from a global perspective. Our observations are drawn from recordings at five different arrays (Table 1), and sample D'' at the geographic regions shown in Fig. 2. Some of the source-and-array combinations used in this study have been published in previous studies (Thomas *et al.* 2004a,b, 2011; Kito *et al.* 2007; Chaloner *et al.* 2009), while data for the Pacific and Bering Sea have not previously been published.

Array processing methods are based on the assumption that the component seismic stations of the array are sufficiently closely spaced that incoming energy from a teleseismic event arrives as a plane wave. By stacking the seismic traces of the stations with a time-shift proportional to the predicted traveltimes between the stations for a given slowness and backazimuth, it is possible to map both the directionality and slowness of seismic energy arriving at the stations. Slowness measurements are critical for determining the bottoming depth of the incoming phases, and thus verifying that PdP and SdS phases come from D'' and not near-source or near-receiver scatterers (e.g. Weber 1993; Thomas *et al.* 2002). In Fig. 3, we show examples of vespagrams (slowness versus traveltimes stacks for a fixed backazimuth) from each of our studied geographic regions (Table 1), in which PdP and SdS phases are clearly visible, with a slowness and arrival time in between the P and PcP phases (or S and ScS phases). While in some cases PdP or SdS may be detected with a linear vespagram, in most cases fourth root vespagrams (Muirhead & Datt 1976) are required to distinguish the phases clearly (Fig. 3). The fourth root vespagram is a non-linear stacking technique, which enhances the visibility of small-amplitude signals through suppression of non-Gaussian noise. For small arrays it gives the same result as a more physically based stacking approach such as the phase weighted stack of Schimmel & Paulssen (1997) and Rost & Thomas (2002).

For each of the regions plotted in Fig. 2, we studied a large number of events and retained only those which displayed a high signal-to-noise ratio in their vespagrams (as illustrated in Fig. 3), typically 10 or more events for each of PdP and for SdS. By 'high signal-to-noise ratio' we mean that the amplitude of the P (or S) wave relative to ambient noise should be greater than 3 (in practice it is usually much higher than this). Additionally, we visually inspected each vespagram and retained only those in which the arrivals had a clear onset and few or no multiples. We also used deep events (i.e. greater than ~ 200 km) in order to have an impulsive P (or S) waveform. Since the vespagrams were calculated for a fixed azimuth, assuming that seismic energy travelled along the great circle path between source and receiver, deviations of seismic energy from the great-circle path due to scattering could theoretically produce peaks in the vespagram with erroneous slowness values (Rost & Thomas 2002). Therefore, we employed the slowness-backazimuth method of Weber & Wicks (1996) and Kaneshima & Helffrich (1998) to verify that the slownesses of the PdP and SdS phases do indeed correspond to waves which had their turning point at D'' depths.

2.1 New data sets

In addition to already published data sets for the Caribbean, Eurasia and Southeast Asia, we also use results from previously unpublished data for regions beneath the Pacific and the Bering Sea. The source-receiver combinations for these regions have reflection points of PdP and SdS waves in tomographically slow areas, compared with the reflection points underneath the Caribbean, Siberia and Southeast Asia, which usually coincide with fast regions in tomography models (e.g. Grand 2002).

For the Bering sea, we use events in Japan and Izu Bonin region recorded at the Northwestern Territories stations (NWT) and stations in British Columbia (BC) of the POLARIS network (Portable Observatories for Lithosphere Analysis and Research Investigating Seismicity, operated by the Geological Survey of Canada). Events from 2003 to 2006 with an epicentral distance range from 60 to 80° and a minimum magnitude (mb) of 5.7 proved most useful. Some events recorded at NWT could not be used for the BC network and vice versa due to a limited number of stations, large epicentral distances (larger than 80°) or noise, which leaves us with 22 individual measurements. The data are filtered with a butterworth bandpass filter between 1 and 10 s (or 2–10 s) for P waves and between 3 and 25 s for S waves. We tried other filters as well but the above-mentioned filters proved the most useful. Each event has been stacked in the vespa process using the theoretical backazimuth for the central station and a range of slowness values suitable for the wave type (i.e. P or S wave). For S waves only the transverse component is used in order to avoid contamination with converted P- to S waves and SKS. Most events showed clearer P-wave arrivals than S-wave arrivals; this is likely due to unfavourable radiation patterns for the S waves which make it difficult to detect S-wave arrivals. However, in the few events where SdS can be seen, its polarity tends to be less ambiguous than that of the PdP phase.

Fig. 4 shows the sources, stations, reflection points in D'', and two examples for P waves as well as one example for S waves used for the Bering Sea region. We verify that the signal between P and PcP (S, ScS) arrives with the correct slowness and backazimuth values for a D'' reflection by using slowness-backazimuth analyses (see e.g. Rost & Thomas 2002).

For the region beneath the Pacific we use similar source-receiver combinations to Avants *et al.* (2006). Events in the Tonga-Fiji region with epicentral distances from 76 to 82°, and depths below 100 km, recorded at Anza (AZ) and the Californian Institute (CI), were collected between 1998 and 2006 (Fig. 5). We use 20 events for P and 20 events for S waves. Figs 5(b)–(d) shows data examples for these events. The data have been filtered with butterworth bandpass filters with periods as given above, and cross-correlated with the P (or S) wave to study the polarity of the D'' reflections. Vespagrams of each event are produced using the theoretical backazimuth of the central station. In all the events with possible PdP and SdS phases, we also verify that the slowness and backazimuth of the PdP and SdS phases are consistent with being generated by a D'' reflection rather than a near-source reflection by using slowness-backazimuth analysis. A positive peak of a PdP (SdS) phase indicates a positive correlation of a phase with the polarity of the P (or S) wave, and vice-versa.

2.2 Polarity measurements

The fourth root vespagram distorts the shape of signal waveforms but preserves their polarity. For our high-quality events, we compared the polarity and number of peaks of the P, PdP and PcP phases (and likewise S, SdS and ScS phases). The relationship between waveform polarities of these phases and the sign of the velocity jump at D'' has been demonstrated by synthetic waveform modelling, for example, by Weber (1993) and Kito *et al.* (2007). On the basis of this modelling, we infer a positive impedance contrast (i.e. an increase in velocity across the reflector) where the waveform polarities are the same for PdP and PcP (or SdS and ScS), and a negative impedance contrast, thus a decrease in seismic velocity across the reflector, where the PdP (or SdS) has the opposite polarity to PcP (or ScS).

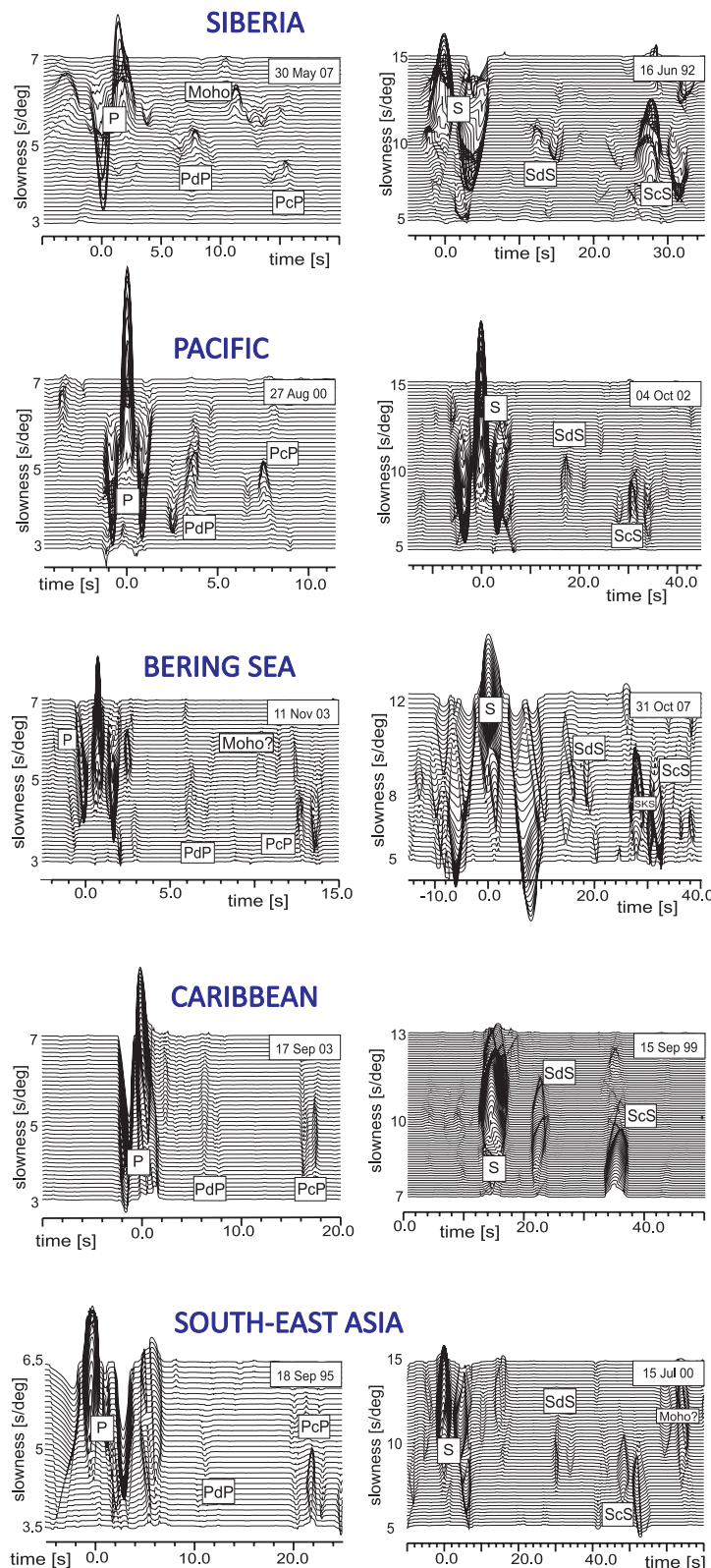


Figure 3. Examples of P - and (transverse) S -component vespagrams (left-hand and right-hand columns, respectively) for the five study regions. Vespagrams are stacked at a fixed backazimuth corresponding to that of the great circle path between event and the receiver at the centre of the array, and are fourth root vespagrams (Muirhead & Datt 1976). Data have been filtered at the following periods: Siberia $P = 1\text{--}10$ s; $S \geq 3$ s; Pacific $P = 1\text{--}5$ s, $S = 3\text{--}25$ s; Bering Sea $P = 1\text{--}10$ s, $S = 3\text{--}25$ s; Caribbean $P = 2\text{--}50$ s, $S \geq 3$ s; Southeast Asia $P = 2\text{--}10$ s, $S = 3\text{--}40$ s. In all examples, the SdS waveform has the same polarity as the ScS . In Siberia, the Pacific and the Bering Sea, the PdP waveform has the same polarity as the PcP waveform, whereas in the Caribbean and Southeast Asia it has the opposite polarity. Arrivals with the same slowness as the P or S waveform are probably Moho multiples.

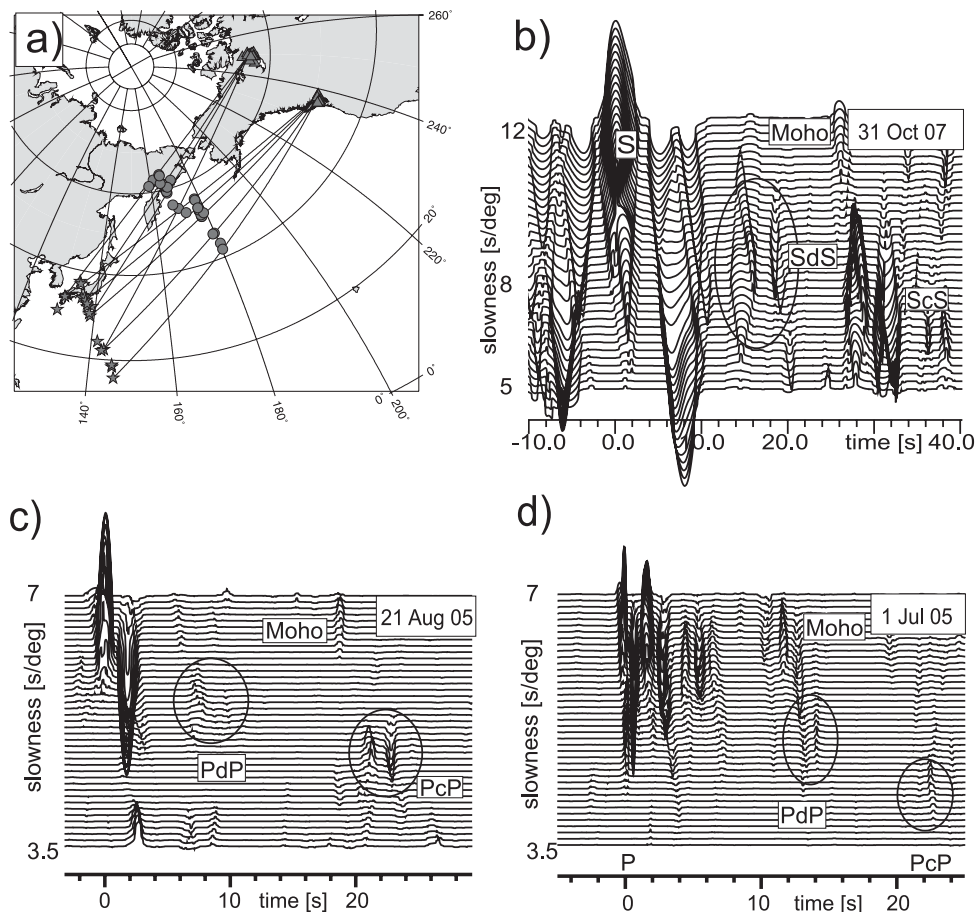


Figure 4. (a) Sources (stars), receivers (triangles) and D'' reflection point (circles) for the Bering Sea region. (b) An example for an S-wave reflection (2007 October 31 recorded at BC stations). SdS is indicated by the circle. The S-wave data have been filtered with a bandpass filter of 3–25 s. (c) and (d) show examples for P-wave reflections: the 2005 August 21 event recorded at NWT stations and the 2005 July 1st event recorded at NWT stations. The P-wave data are filtered with a bandpass filter of 1–10 s.

We find that *within* each of our study regions, the inferred polarity of the D'' reflection is the same for the majority of events (e.g. see the event compilation in table 1 of Chaloner *et al.* (2009) for Southeast Asia). While our SdS observations always have a positive polarity across all regions, PdP displays both positive and negative polarities, depending on the geographic region (Table 1). It is unlikely that a polarity reversal in PdP relative to P and PcP would arise from focal mechanism effects, that is, having a ray path which travelled through a different quadrant of the focal sphere from the P and PcP, because the P and PcP have the same polarity as each other. The take-off angle of the PdP phase lies between the P and PcP, and the fact that the latter have the same polarity indicates that they originated within the same quadrant of the focal sphere. In the Bering Sea, the PdP phase is typically weak in amplitude, and it is more difficult to assign an average polarity than in the other four regions. We interpret most Bering Sea events as showing a positive PdP polarity, but this is more uncertain than for the other regions.

2.3 Amplitude measurements

We use the reflectivity method of Müller (1985) to calculate synthetic seismograms for various 1-D earth models with different magnitude velocity jumps across the D'' reflector. These synthetic seismograms are processed in an identical manner to the real data, and the resulting fourth root vespagrams are compared with the real data vespagrams. In particular, we measure the relative amplitude

of the PdP waveform to that of the P waveform (and SdS relative to S). Although waveform amplitudes are, by definition, modified during the computation of fourth root vespagrams, by measuring relative rather than absolute amplitudes, and subjecting all data to the same processing steps, comparison between real and synthetic data is plausible.

We assume that the amplitude ratios in the real data depend primarily on the magnitude of the velocity jump at D'', and compare real with synthetic vespagrams to estimate a range of velocity jumps across the reflector which are consistent with the real data. In reality, PdP and SdS amplitudes are influenced by multiple factors, such as 3-D topography on the reflecting surface, scattering along the wave path, attenuation and anisotropy. These factors are not included in our synthetic modelling because at present, full 3-D waveform modelling at the high frequencies corresponding to D'' reflections is computationally difficult. Additionally, the magnitude of the velocity jump across the discontinuity trades off (inversely) with the vertical thickness of the discontinuity (Weber 1993). Thus, the ranges of the velocity jumps given in Table 1 have a large uncertainty, and should not be subjected to overinterpretation. Although we cannot place absolute uncertainties on the estimated velocity jumps, synthetic modelling indicates that a velocity jump of at least 1 per cent is required for a PdP or SdS phase to be visible above the noise levels (Weber 1993; Kito *et al.* 2007; Chaloner *et al.* 2009), so we can confidently place this as a lower bound on the magnitude of the jump.

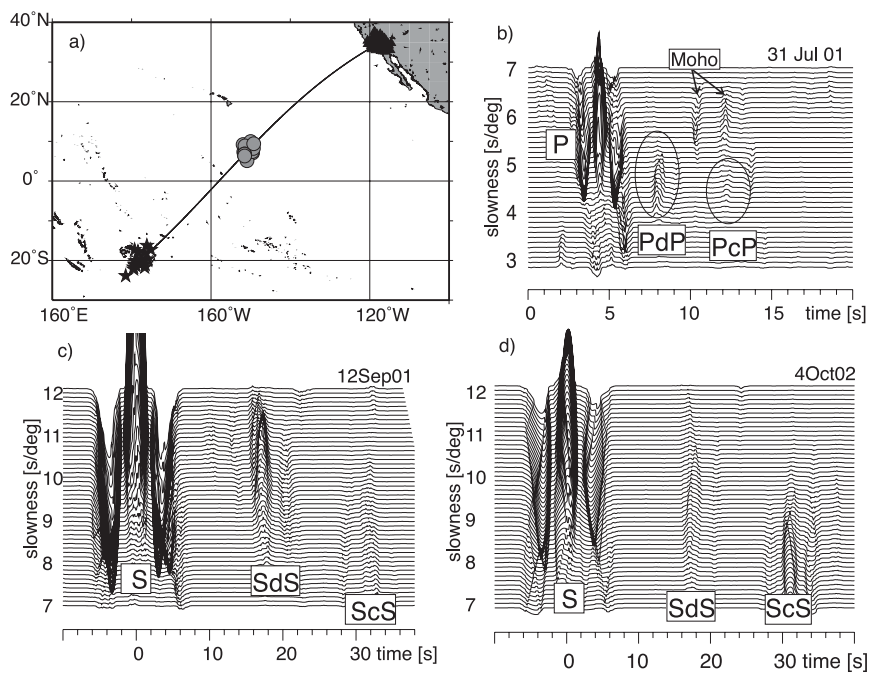


Figure 5. (a) Sources (stars), receivers (triangles) and D'' reflection points (circles) for the investigation of the Pacific region. (b) An example of a P -wave reflection at D'' (2000 August 27). The event has been filtered with a bandpass filter from 1 to 5 s and the traces have been cross-correlated with the P wave. (c) and (d) show examples for S -wave reflections from the D'' region, for events on 2001 September 12 and 2002 October 4. The data have been bandpass filtered from 3 to 25 s and cross-correlated with the S -wavelet.

2.4 Compilation

Our polarity and amplitude measurements for each study region are averaged over the available high-quality events and the inferred velocity jumps at the D'' reflector are summarized in Table 1. Implicit in our method is the assumption that within each region, the structure of the D'' reflector is sufficiently homogeneous, that it is reasonable to take the average of the polarity and amplitude measurements for multiple events. Furthermore, we assume that P and S waves are sampling approximately the same structures (albeit with different Fresnel zones and frequency sensitivity). While these assumptions cannot be verified due to data quality, for the good quality data, approximately 80–90 per cent of the polarity and amplitude measurements are in agreement at each region, and we believe this level of agreement is sufficient as an introductory step towards constraining the origin of D'' reflections. The advantage of our method is that all the seismic data from different regions have been subjected to the same array processing methods, and have consistently applied thresholds for defining a good signal-to-noise ratio. Only high-quality data are retained in the analysis.

3 MINERAL PHYSICS MODELLING OF D'' REFLECTIONS

We consider two alternative explanations for D'' reflections: (1) scattering off thermochemical heterogeneity and (2) a sharp impedance contrast due to a phase change from perovskite to post-perovskite. In the former case, we focus particularly on the generation of reflections by subducted material. We assume isotropic mineralogical structures in all our calculations. Anisotropy remains a plausible and important additional candidate for D'' reflections (Thomas *et al.*

2011) but is beyond the scope of this study; future investigation of its effects is warranted.

Since we are comparing different classes of models, it is not our goal to find an exact or unique solution for the physical structure which generates D'' reflections, but rather to examine which class of models, if any, is more likely to contribute to the generation of D'' reflections. The sensitivities of V_p and V_s with respect to individual thermochemical parameters (temperature, Fe content, pV content, etc.) have previously been calculated and are presented in Deschamps *et al.* (2012). However in the real Earth, it is likely that multiple thermochemical parameters change simultaneously across the D'' discontinuity. The purpose of this study is to investigate the overall change in V_p and V_s when these parameters are simultaneously changed in an amount and direction that is compatible with a particular explanation for D'' structure.

Our procedure for modelling D'' seismic structure in terms of thermochemical structure is shown schematically in Fig. 6. We assume that above the discontinuity (starting model), the mantle has a mineralogy M_1 and temperature T_1 . Below the discontinuity (end model), the mineralogy is M_2 and temperature is T_2 . For each of these models, seismic velocities V_p and V_s are computed using the elastic parameters and equation of state of Stixrude & Lithgow-Bertelloni (2011), and a Voigt–Reuss–Hill averaging scheme to calculate the average velocity for mineral aggregates. Velocities are not corrected for attenuation since the seismic effect of attenuation is believed to be negligibly small in the lower mantle (Brodholt *et al.* 2007). The velocity above the discontinuity (V_1) is subtracted from the velocity below the discontinuity (V_2), and we observe first whether the sign of $V_2 - V_1$ (i.e. positive or negative) agrees with the waveform polarities of our seismic observations in Table 1. If the polarities agree, we then observe whether the magnitude of $V_2 - V_1$ agrees with the ranges of

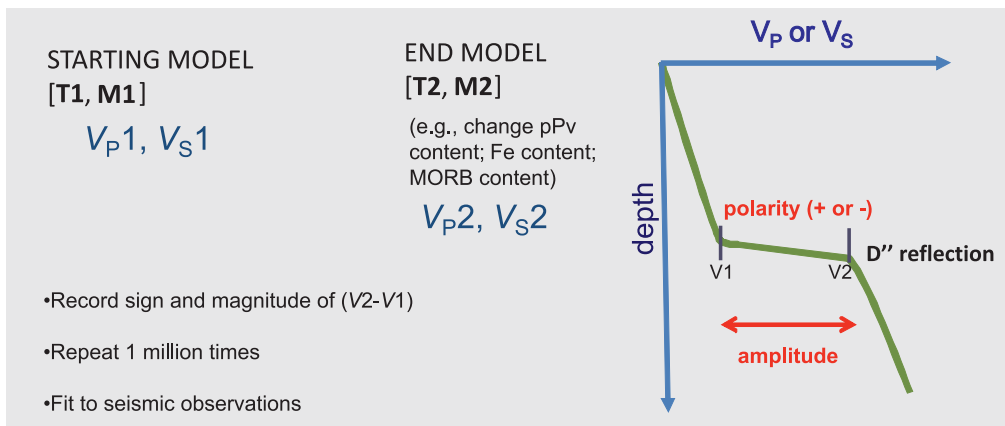


Figure 6. Schematic diagram illustrating our procedure for fitting seismic observations of a D'' discontinuity with a particular thermochemical structure. T , temperature; M , mineralogy. The sign of $V_2 - V_1$ is compared with waveform polarity measurements and the magnitude of $V_2 - V_1$ is compared with amplitude measurements (listed in Table 1).

velocity jumps inferred from our amplitude observations, as given in Table 1.

There are three main sources of uncertainty in the mineral physics calculations: (1) experimental uncertainties on the mineral elastic parameter values, needed to compute seismic velocities (i.e. bulk modulus, shear modulus, density, and their temperature and pressure derivatives); (2) plausible mantle compositions and temperatures at D'' depths, and (3) the degree of chemical heterogeneity (0–100 per cent), phase change (0–100 per cent) or temperature change required to generate D'' reflections, including trade-offs between these parameters and factor (2). In order to take these uncertainties into account, for each D'' hypothesis which we test (i.e. phase change in perovskite; scattering off subducted material, etc.) we allow both the elastic parameters and thermochemical composition to vary within specified ranges rather than assuming fixed values. Chemical ranges are listed in Tables 2–4, and elastic parameters vary within the uncertainty bounds published in table A1 of Stixrude & Lithgow-Bertelloni (2011). We then generate 1 million models whose elastic parameters, mineralogy and temperature lie within these bounds, the precise values for each model being chosen at random in a Monte Carlo procedure. Monte Carlo modelling of

Table 2. Compositional ranges of MORB models (CM) in this study, taken from Deschamps *et al.* (2012), and based upon the MORB compositions published in Hofmann (1988), Irfune & Ringwood (1993), Ono *et al.* (2001, 2005), Ricard *et al.* (2005), Perrillat *et al.* (2006) and Ricolleau *et al.* (2010). For each model, volume percentages of MgSiO₃, FeSiO₃, CaSiO₃ and Al₂O₃ are chosen at random from a uniform distribution between the minima and maxima given in this table. The volume percentage of SiO₂ is then set to 100 minus the sum of the other components, but the model is only used if the SiO₂ content is between 12 and 22 per cent.

Mineral	Min (vol per cent)	Max (vol per cent)
MgSiO ₃	21.0	28.1
FeSiO ₃	12.0	19.0
CaSiO ₃	23.8	28.6
Al ₂ O ₃	16.7	17.9
SiO ₂	100 minus sum of above components, but restricted to the range 12–22 per cent	

Table 3. Compositional ranges of non-MORB mantle component (CN) when generating D'' reflections via a change in MORB content, based upon expected ranges for harzburgitic and pyrolytic mantle. For every model, each of the parameters A to E is selected at random from a uniform distribution between the maxima and minima given in this table. F is fixed to 100-E to ensure that the total volume adds up to 100 per cent.

Compositional Parameter	Lower bound	Upper bound
(A) Vol per cent (Mg,Fe)SiO ₃ +(Mg,Fe)O	90	100
(B) Vol per cent (Mg,Fe)SiO ₃ within (A)	70	100
(C) Vol per cent FeSiO ₃ within (B)	0	20
(D) Partition coefficient Fe-Mg between (Mg,Fe)SiO ₃ and (Mg,Fe)O	0.1	0.6
(E) per cent CaSiO ₃ within non-(Mg,Fe)-bearing minerals	0	100
(F) per cent Al ₂ O ₃ within non-(Mg,Fe)-bearing minerals		100-E

Table 4. Compositional ranges applied when testing seismic properties of synthetic D'' reflector structure due to a phase change in perovskite, or change in iron or perovskite content, based upon expected ranges for pyrolytic mantle, harzburgitic mantle or a mixture of MORB plus one of these components. For every model, each of the parameters A to F is selected at random from a uniform distribution between the maxima and minima given in this table. G is fixed to 100 – (E+F) to ensure that the total volume adds up to 100 per cent.

Compositional Parameter	Lower bound	Upper bound
(A) Vol per cent (Mg,Fe)SiO ₃ +(Mg,Fe)O	85	100
(B) Vol per cent (Mg,Fe)SiO ₃ within (A)	70	100
(C) Vol per cent FeSiO ₃ within (B)	0	20
(D) Partition coefficient Fe-Mg between (Mg,Fe)SiO ₃ and (Mg,Fe)O	0.1	0.6
(E) per cent Al ₂ O ₃ within non-Mg,Fe minerals i.e. CaSiO ₃ +Al ₂ O ₃ +SiO ₂ component	0	100
(F) per cent SiO ₂ within CaSiO ₃ +Al ₂ O ₃ +SiO ₂ component	0	100
(G) per cent CaSiO ₃ within CaSiO ₃ +Al ₂ O ₃ +SiO ₂ component		100-(E+F)

thermochemical and mineral physics parameters is an established procedure for assessing uncertainties (e.g. Trampert *et al.* 2001, 2004; Deschamps & Trampert 2003; Cammarano *et al.* 2005; Cobden *et al.* 2008, 2012; Deschamps *et al.* 2012). Although the model space of the uncertainties is large, previous studies have verified that the full distribution of seismic properties is adequately represented by a sample size of 1 million models (e.g. Deschamps *et al.* 2012). We assume a uniform distribution of both the chemical and mineral elastic parameters within their permitted ranges, in other words, every value between the maximum and minimum is equally likely. Furthermore, since both the average temperature and the likely magnitude of lateral and vertical variations in temperature at the D'' discontinuity are relatively unconstrained, we assume a uniform distribution of temperatures between a specified minimum and maximum value. Of the 1 million models, we compute how many fit the waveform polarities for both PdP and SdS, and how many fit the polarities and amplitudes simultaneously, for each of the five study regions in Fig. 2 and Table 1. By ‘fitting polarities and amplitudes’, we of course mean that the sign of the velocity jump will generate the same waveform polarity as the seismic observations, and the magnitude of the jump would generate the same waveform amplitudes as the seismic observations.

As we will show in the results sections (Section 4–6), significant differences in the number of fitting models occur for the five geographic regions, and can be interpreted as a statistical measure of the relative likelihood that a particular physical structure is the cause of D'' reflections. We consider the fit of polarities both in isolation and in combination with the amplitude measurements, because the latter have large uncertainties, so our interpretation of amplitude measurements is correspondingly cautious. Modelling PdP and SdS simultaneously is essential for distinguishing the relative fit of different thermochemical structures.

Variations in composition across the D'' discontinuity are expressed as changes in the volume percent of the component minerals. We include the following minerals in our calculations: perovskite ($MgSiO_3$, $FeSiO_3$, Al_2O_3), post-perovskite ($MgSiO_3$, $FeSiO_3$ and Al_2O_3), magnesiowustite (MgO , FeO), calcium perovskite ($CaSiO_3$) and free silica (SiO_2). SiO_2 is present as the high-pressure α - PbO_2 structure, seifertite, which is expected to occur at D'' depths (Murakami *et al.* 2003), although the differences in seismic properties between seifertite and other high-pressure polymorphs are small according to our database. Modelling of phase equilibria for given chemical composition is not implicitly included in our calculations. This leads to the possibility that some thermodynamically unstable mineral assemblages may be generated, which in turn may produce ‘false positives’ in terms of what fits the seismic data. (It does not, of course, produce false negatives of what does not fit the seismic data.) However, in the case of chemical heterogeneity, there may be mechanical mixing between structures with different chemical compositions, such that the bulk average mineralogy does not conform to the thermodynamically stable mineral assemblage. Furthermore, the nature of the phase boundary between perovskite and post-perovskite remains controversial (e.g. Ohta *et al.* 2008; Catalli *et al.* 2009; Andrault *et al.* 2010), and we wish to test the fit of the seismic data to the mineral elastic properties without pre-conditioning the solution based on a subset of the sometimes-contradictory experimental observations. We ensure that our models are at least partially grounded in physical reality by restricting the seismic velocity at the top of the D'' reflector to lie within ± 5 per cent of the 1-D reference model AK135 (Kennett *et al.* 1995). This is about two to five times the maximum amplitude of velocity perturbations present in lower mantle tomography

models (e.g. Karason & van der Hilst 2001; Grand 2002; Ritsema *et al.* 2011; Mosca *et al.* 2012), which in turn likely underestimate the amplitude of lateral velocity variations at the scale of D'' reflectors. This restriction, together with limiting the ranges of mineralogical compositions to be based around compositional models from petrology (Tables 2–4), minimizes the possibility that our final interpretation is biased by the presence of thermodynamically unstable mineral assemblages.

Seismic velocities V_2 and V_1 are calculated at a fixed depth of 2600 km (119 GPa). In other words, we assume that D'' reflections are generated by a discontinuous increase in velocity at a single, fixed depth. In practice, D'' reflectors likely have a laterally variable depth and thickness. However, we find that this simplification does not bias our interpretation, because the sensitivity of seismic velocities to changes in depth of up to ± 200 km (the maximum expected variation in D'' topography, e.g. Wysession *et al.* 1998) are an order of magnitude smaller than the sensitivity to changes in temperature and composition (illustrated in Deschamps *et al.* 2012).

4. D'' REFLECTIONS FROM SUBDUCTED MATERIAL

Subducted lithosphere consists of a mid-ocean ridge basaltic crust (MORB) of ~ 7 km thickness underlain by ~ 90 km of harzburgitic material. In the lower mantle, the seismic properties of harzburgite are similar to that of pyrolite (Cobden *et al.* 2009), with the latter usually assumed to represent the average mantle chemical composition, approximately. However, basalt is seismically distinct from both pyrolite and harzburgite due to its being silica-saturated and thus lacking a magnesiowustite $[(Mg,Fe)O]$ phase. Therefore, we expect that seismic reflections related to subducted material most likely arise from the basaltic component, and we parametrize D'' reflections from subducted material as a change in basalt (MORB) content between M_1 and M_2 . Since basalt comprises only a minority component of subducted lithosphere, we allow the change in basalt content across the reflector to vary between 0 and ± 100 per cent, assuming that vertical variations in its concentration will depend upon the amount of slab deformation or crustal delamination which has occurred.

Significant variations in the precise chemical composition of MORB have been documented (see references in Table 2). We adopt the parametrization of Deschamps *et al.* (2012) for expressing the observed natural variety in MORB composition as uncertainties in mineral abundances within MORB (listed in Table 2). Above and below the D'' reflector, we model M_1 and M_2 as a mechanical mixture between a MORB component (CM), whose composition is chosen at random from the ranges given in Table 2, and a non-MORB component (CN), whose composition is chosen at random from the ranges given in Table 3. While CM and CN are different for each of the 1 million simulations, within one simulation their mineralogies are fixed above and below the reflector, and it is the ratio of CM to CN, which changes across the reflector. CM and CN are chosen at random such that each can lie between 0 and 100 per cent, and $CM + CN = 100$ per cent, above and below the discontinuity.

If the subduction process is still active, the subducted material may be colder than the ambient mantle, whereas if subduction is no longer active but basaltic material has accumulated at the CMB through excess density (e.g. Christensen & Hofmann 1994; Nakagawa & Tackley 2004; Hirose *et al.* 2005; Ono *et al.* 2005), it may be hotter than the surroundings. Physical constraints on the amplitude of lateral and vertical temperature variations at D'' depths are

limited; we initially give T_1 and T_2 in our models the freedom to vary between 1400 and 3400 K, which is approximately equal to the temperature expected for a 1573 K (1300 °C) adiabat at 2600 km, plus or minus 1000°. This allows temperature variations across the D'' reflector of up to 2000°, probably unrealistic, but since both T_1 and T_2 are chosen at random from a uniform distribution between 1400 and 3400 K, smaller temperature variations occur most frequently (Fig. 7, left).

In Fig. 7, we show the fit of the 1 million models to the waveform polarities and amplitudes in each geographic region. We show the results in 2-D graphical form (as opposed to numerically) so that the trade-off between changes in temperature and changes in chemical composition can be observed. Additionally, the 2-D plots allow us to see the frequency distribution of changes in MORB content, that is, if a particular percentage change in MORB content is preferred for fitting the data.

We note that far more models—by an order of magnitude—fit the polarities in regions where PdP is positive (Siberia, Pacific and Bering Sea) than where it is negative (Caribbean, Southeast Asia). There is a slight tendency in all regions to favour models with an increase in MORB content, and a larger tendency to favour models in which temperature decreases on the underside of the reflector. Regarding amplitudes, no models fit both the polarities and amplitudes in the Caribbean, and only 35 from 1 million are left for Southeast Asia. More than 20 000 models remain in Siberia and the Pacific, but their physical properties are most frequently characterized by a large decrease in temperature (600–1000 K) rather than large changes in MORB content (the modal change being ±0–10 per cent).

We feel that the seismic fit of the models in Fig. 7 is dominated by changes in temperature rather than MORB content, so we then re-ran the simulations but imposed a fixed temperature across the reflector, that is, $T_1 = T_2$ (Fig. 8). The relative fits of the waveform polarities and amplitudes in the different regions are similar to before—that is, significantly better fit in regions with a positive PdP —but it is much clearer now that: (1) it is possible to fit the observations with a change in MORB alone without concurrent changes in temperature and (2) the data are fit significantly more frequently by an increase in MORB content across the reflector rather than a decrease. In Fig. 8, we show not only the frequency distribution of the models as a function of changes in MORB content, but also of changes in iron (Fe) content. This illustrates that in the cases where models fit the seismic data with a decrease in MORB content (i.e. less MORB on the underside of the reflector than above it), they do so only with a concurrent decrease in iron content. Variations in Fe content stem from uncertainties in the actual composition of both MORB and ambient mantle. Thus, although we have shown that it is possible to fit D'' reflections with an increase in MORB content, such as we might expect for scattering of seismic energy off a pile or layer of subducted basaltic material, we must remain aware that it is not possible to do this for all MORB compositions, particularly the more iron-rich variants.

Since temperature variations of up to 2000 K are most likely unrealistically large, we re-ran the simulations with T_1 and T_2 each able to vary between 1900 and 2900 K, that is, allowing a maximum temperature change across the D'' reflector of 1000 K (Fig. A1). In this case, fitting of seismic observations is more strongly correlated with an increase in MORB content than in Fig. 7, but still significantly correlated with a decrease in temperature.

In Fig. 9, we illustrate why it is difficult or impossible to fit both polarity and amplitude measurements in regions where the PdP polarity is negative. Despite the large uncertainty in inferring

velocity changes across a reflector from amplitude observations, synthetic tests (Kito *et al.* 2007; Chaloner *et al.* 2009) demonstrate that a velocity change of at least 1 per cent is required to produce sufficiently large amplitude reflections that they are visible above the noise level. However, the seismic properties of basalt are such that in order to generate an increase in S-wave velocity, as required by the SdS reflections, a decrease in P-wave velocity of at most 1.2 per cent is possible, which is at the lower limit of what can be detected seismically. This holds with or without a change in temperature accompanying the change in basalt content (Figs 9a and 7b), and for this reason it is difficult to fit waveform amplitudes in the PdP -negative regions via a change in MORB content.

5 REFLECTIONS FROM PEROVSKITE → POST-PEROVSKITE PHASE CHANGE

When modelling D'' reflections with transformation from perovskite to post-perovskite, we select a mineralogy at random from the ranges given in Table 4. We assume that above the reflector, the amount of post-perovskite is zero, and below the reflector, between 0 and 100 per cent of the perovskite (Pv) has converted to post-perovskite (pPv). All other compositional parameters remain unchanged. The percentage of pPv below the reflector is chosen randomly, assuming a uniform distribution between 0 and 100 per cent. We assume that the same percentage of pPv relative to Pv is present for Mg, Fe and Al-perovskite phases. We then study the fit to waveform polarities and amplitudes first in the case where there are concurrent temperature variations across the reflector (T_1 and T_2 each vary at random between 1400 and 3400 K), and secondly in the case where the temperature is fixed across the reflector.

We find that where the temperature is variable (Fig. 10), regions with positive PdP polarity are best fit by models with a decrease in temperature, and a minimal change in post-perovskite content below the reflector, in other words they are fit by temperature changes rather than post-perovskite changes. No models can fit both amplitudes and polarities in the Bering Sea, and those in Siberia and the Pacific mostly require a decrease in temperature of at least 500 K. In regions with a negative PdP polarity, the opposite happens, namely that the larger the increase in post-perovskite content, the greater the number of models which fit the seismic data. There is a slight preference when fitting the amplitudes in these regions to favour models which have an increase in temperature below the reflector rather than a decrease, but in general, models with small to zero change in temperature are the most abundant; in other words, in regions with a negative PdP polarity, the models fit the data primarily due to the effect of post-perovskite rather than temperature. Although the number of models fitting both the amplitudes and polarities is small for these regions (a few hundred), it is clear that there is a strong correlation between the number of models and the size of the post-perovskite increase.

In the simulations with fixed temperature (Fig. 11), the number of models fitting both amplitudes and polarities in PdP -positive regions is dramatically reduced (less than 30 models for Siberia and the Pacific; and just 2 for the Bering Sea). Fig. 12 illustrates why this is the case: for a phase change from perovskite to post-perovskite, increases in P-wave velocity do not exceed 1 per cent with our mineral physics data set, but for our seismic data at least 1 per cent change is required to produce observable PdP reflections above the noise level.

In PdP -negative regions, there is no correlation between the degree of increase in pPv content and number of models when fitting

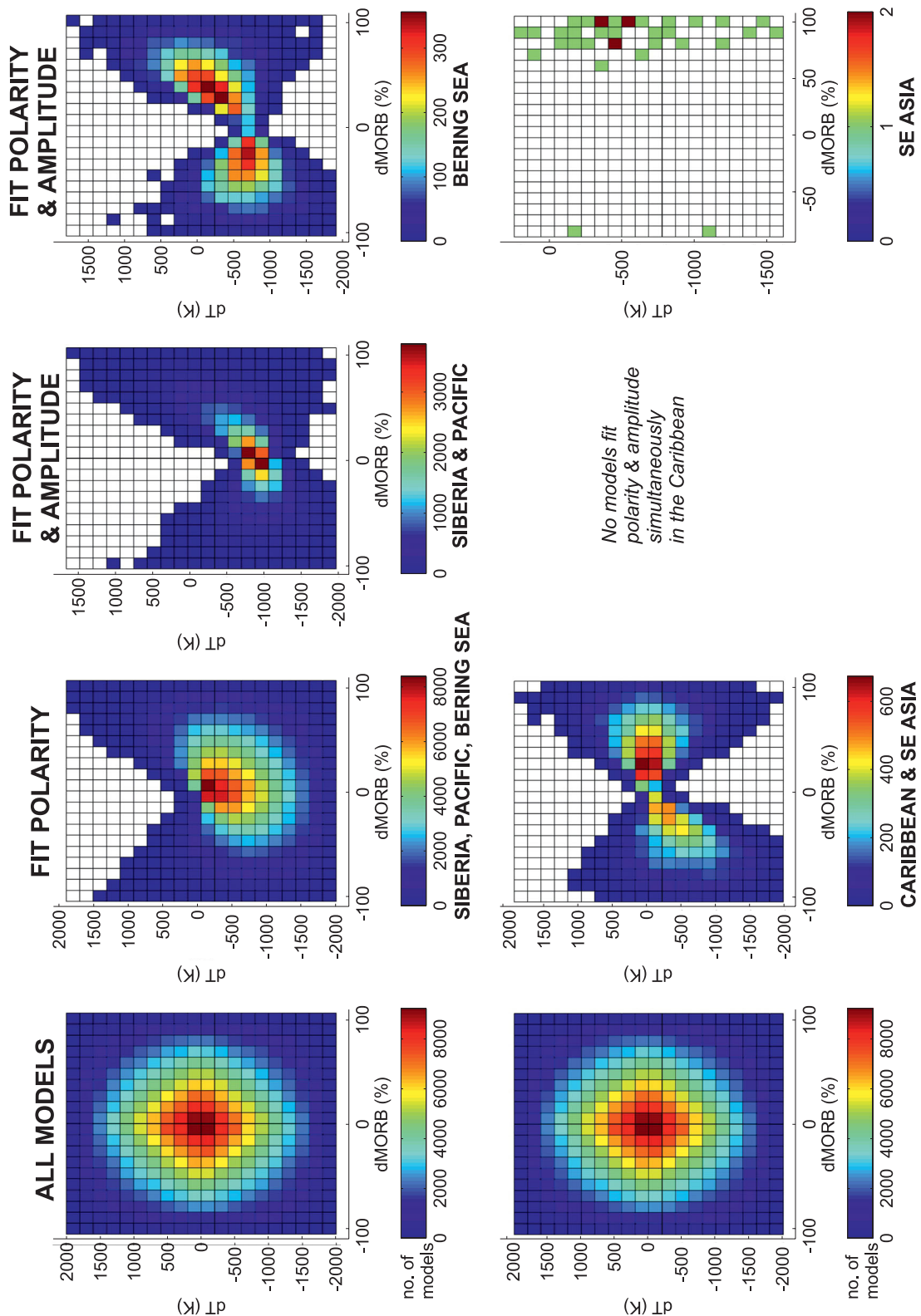


Figure 7. The result of modelling D'' reflections via a change in MORB content with a concurrent change in temperature. We have plotted 2-D frequency distributions showing number of models versus temperature change and change in MORB content from above to below the D' discontinuity. The left-hand column shows the original distribution of 1 million models. The second column shows the distributions of the remaining models after fitting waveform polarities, and the third and fourth columns show the distributions of the remaining models after fitting both polarities and amplitudes in five different regions. Siberia and the Pacific have the same seismic properties according to our data (Table 1) so only one plot is shown for the two regions.

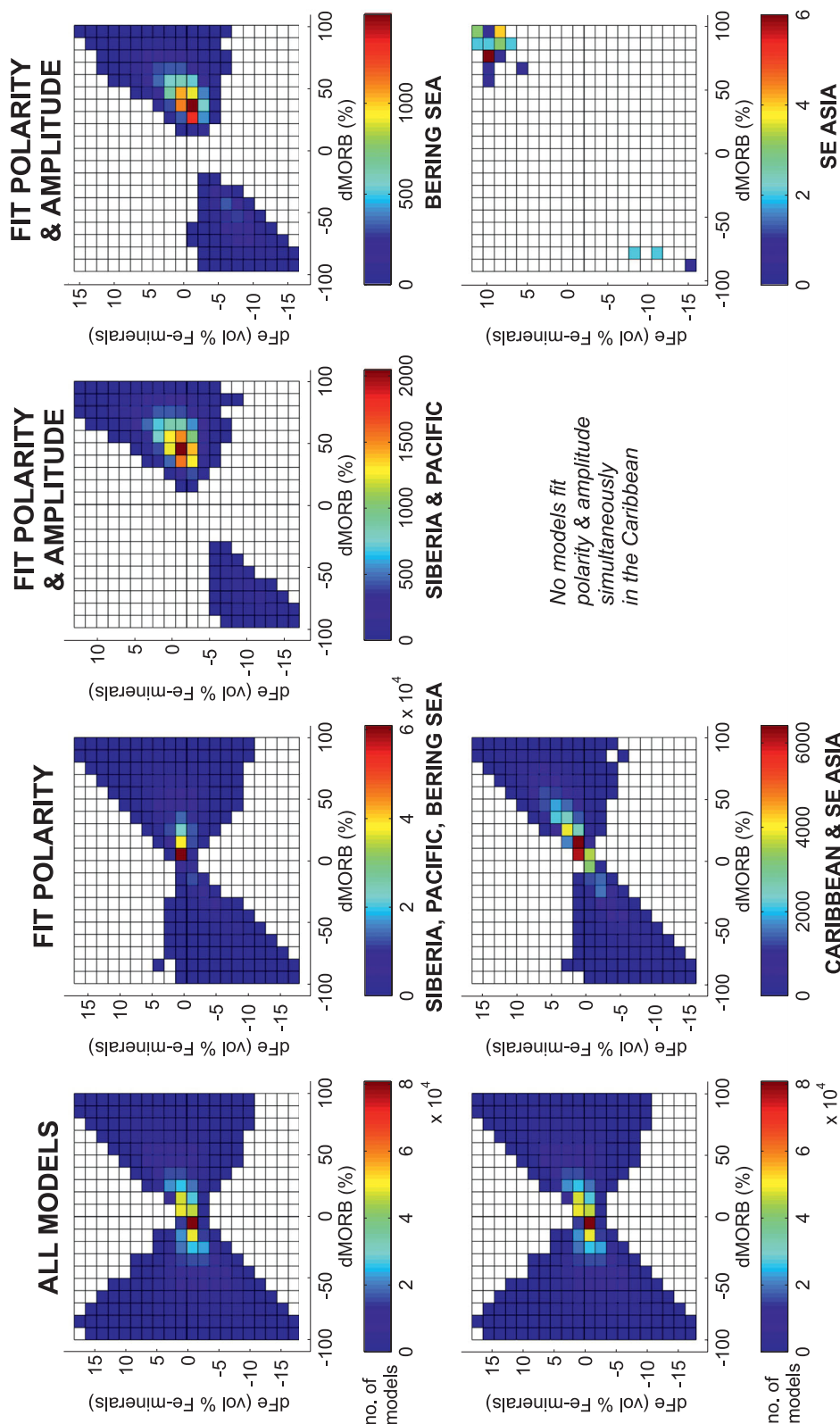


Figure 8. The result of modelling D'' reflections via a change in MORB content and no change in temperature across the discontinuity. We have plotted 2-D frequency distributions showing number of models versus change in MORB content and change in iron content from above to below the D'' discontinuity. Left-hand column shows the distribution for 1 million initial models, other columns show the remaining models after fitting waveform polarities and amplitudes in different regions. Change in iron content is expressed as volume percent change in Fe-bearing minerals, that is, FeSiO_3 and FeO .

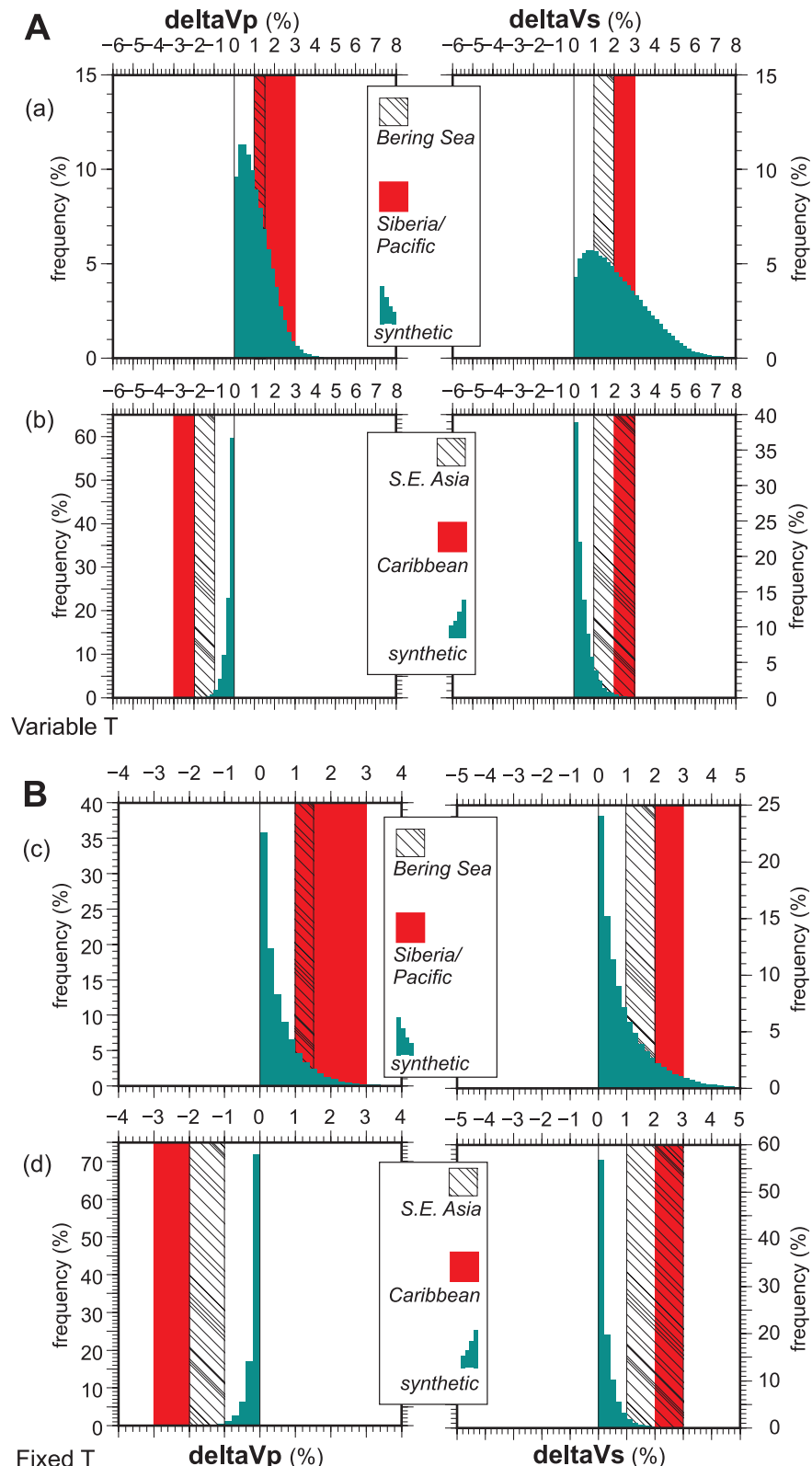


Figure 9. The velocity jump across D'': a comparison between the ranges estimated from seismic observations (solid red bars and black/stripy bars), and the synthetic models, when synthetic models impose a change in MORB content across the D'' discontinuity. Green histograms show frequency distribution of those synthetic models, which have the correct polarity for a particular geographic region. Upper panel (A) shows the results for variable temperature models (i.e. the temperature can change across the D'' discontinuity), lower panel (B) shows the results for models in which temperature does not change across the D'' discontinuity. It is difficult to generate a large amplitude decrease in P -wave speed using MORB and therefore to fit amplitude measurements in Southeast Asia and the Caribbean.

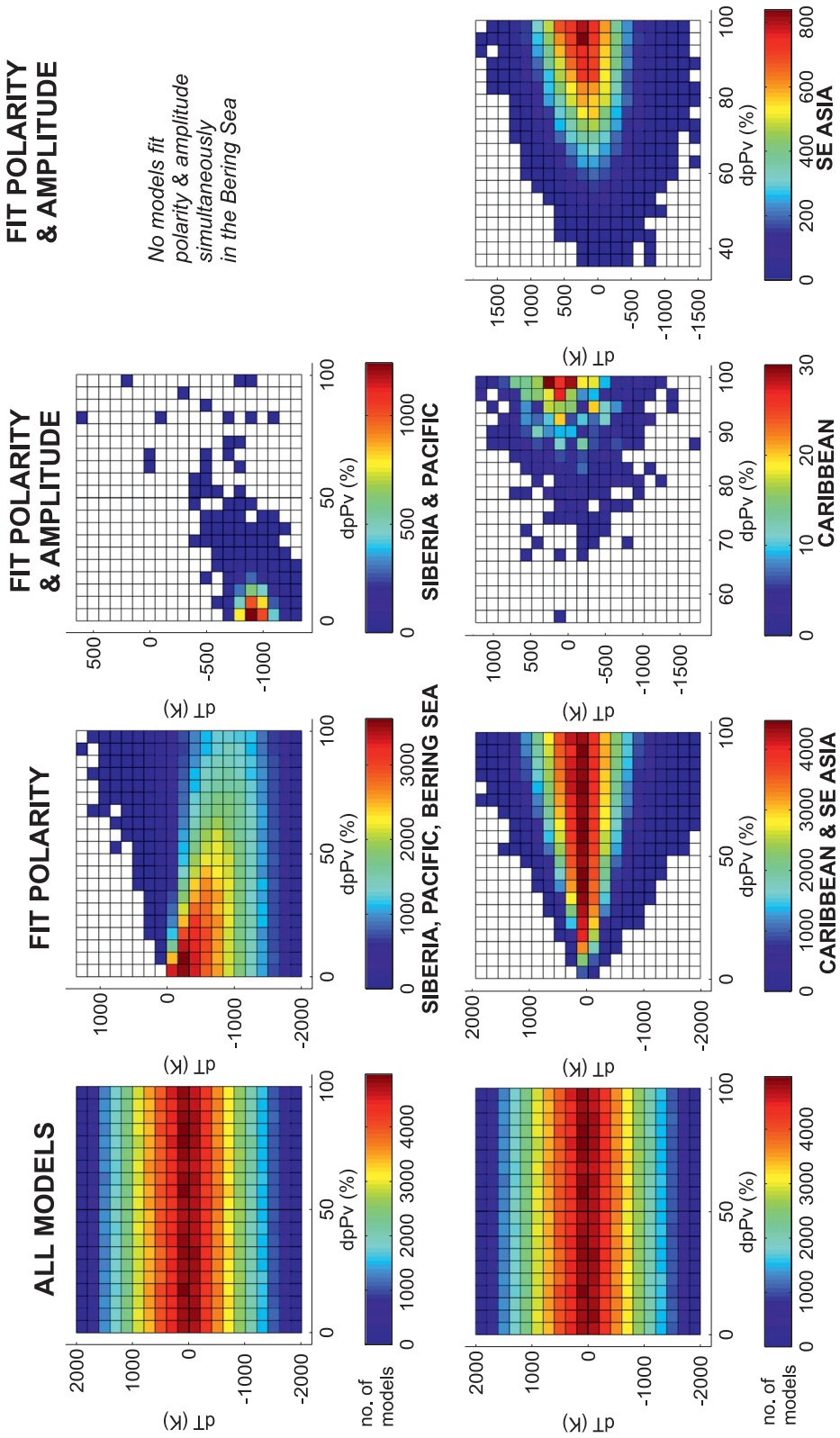


Figure 10. The result of modelling D' reflections via a phase change from perovskite to post-perovskite across the discontinuity, with a concurrent change in temperature. We assume no pV is present above the discontinuity and 0–100 percent conversion of Pv to pV below. We have plotted 2-D frequency distributions showing number of models versus change in pV content and change in temperature from above to below the D' discontinuity. Left-hand column shows the distribution for 1 million initial models, other columns show the remaining models after fitting waveform polarities and amplitudes in different regions. pV content is calculated as the percentage of $(\text{Mg}, \text{Fe})\text{SiO}_3$ present as pV rather than Pv.

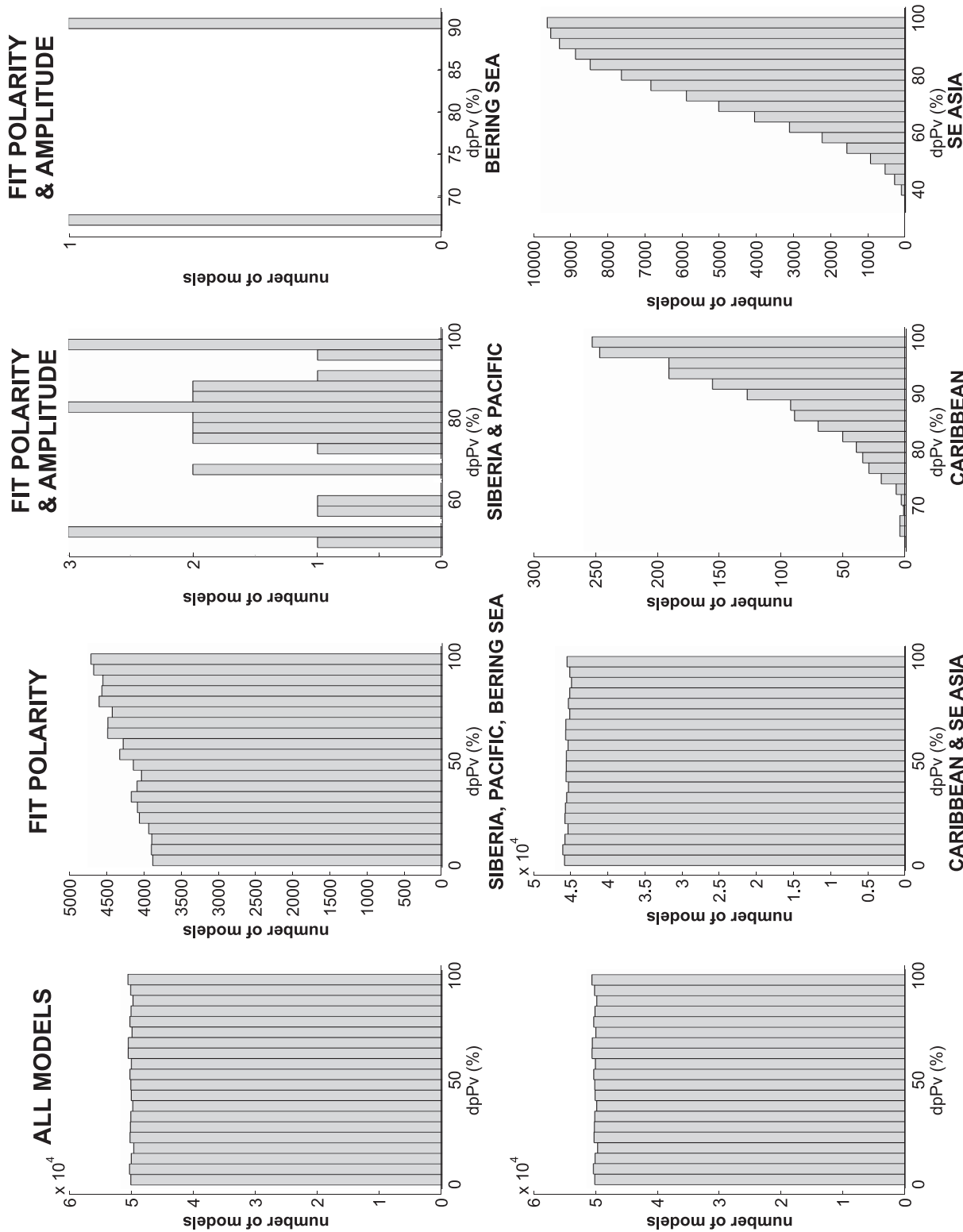


Figure 11. The result of modelling D'' reflections via a phase change from perovskite to post-perovskite assuming no change in temperature across the discontinuity. We show here frequency distributions of the number of models versus change in p_{Pv} content. Left-hand column shows the distribution for 1 million initial models, other columns show the remaining models after fitting waveform polarities and amplitudes in different regions. p_{Pv} content is calculated as the percentage of $(\text{Mg}, \text{Fe})\text{SiO}_3$ present as Pv rather than Pv .

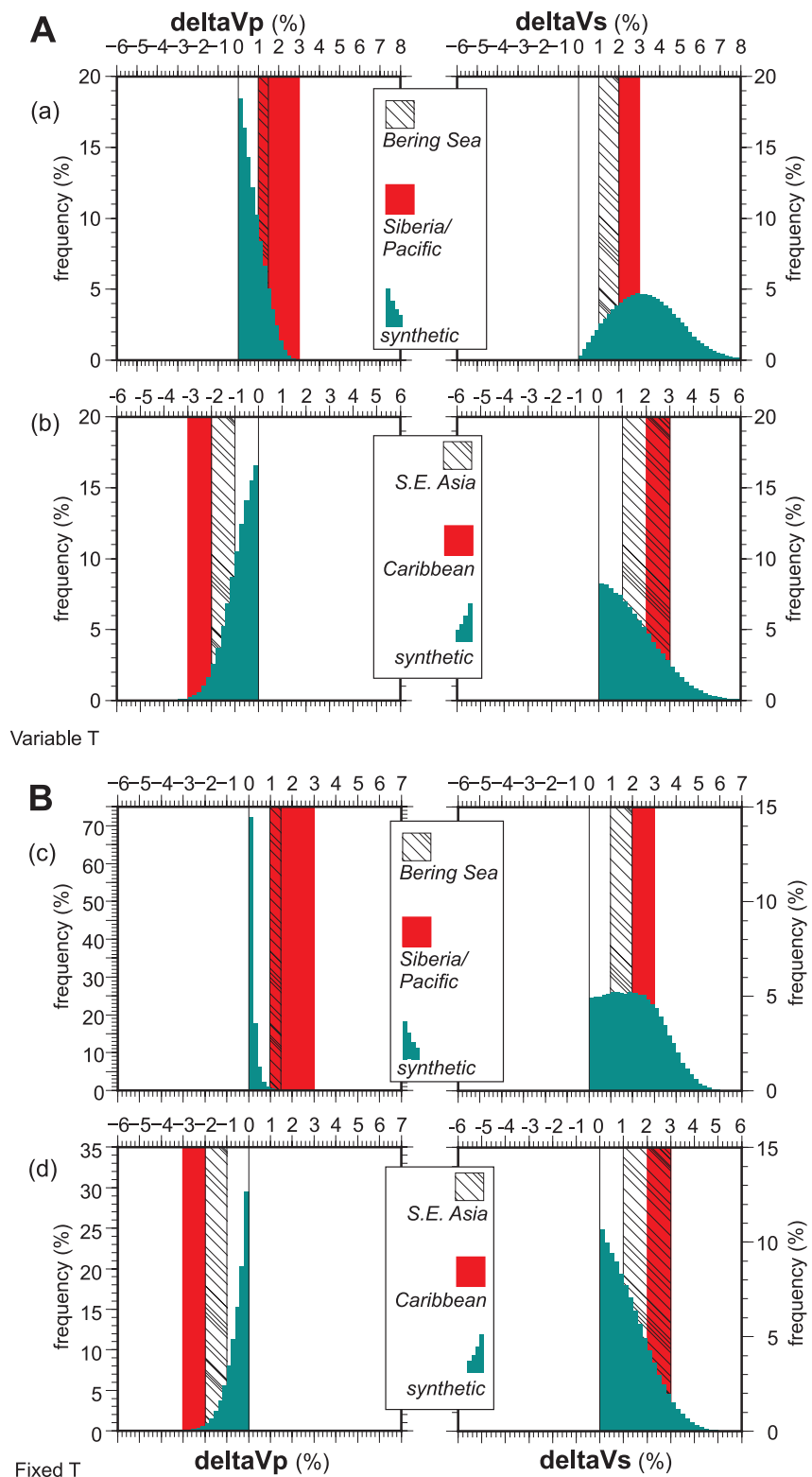


Figure 12. The velocity jump across D'': a comparison between the ranges estimated from seismic observations (solid red bars and black/stripy bars), and the synthetic models, when synthetic models impose a change in post-perovskite content across the D'' discontinuity. Green histograms show frequency distribution of those synthetic models, which have the correct polarity for a particular geographic region. Upper panel (A) shows the results for variable temperature models (i.e. the temperature can change across the D'' discontinuity), lower panel (B) shows the results for models in which temperature does not change across the D'' discontinuity. It is difficult to generate a large amplitude increase in P-wave speed unless there is a concurrent change (decrease) in temperature, and therefore it is difficult to fit amplitude measurements in Siberia, the Pacific and the Bering Sea using purely isotropic post-perovskite.

only polarities (Fig. 11). When considering both polarities and amplitudes, the number of models which can fit the data is larger than in the case where the temperature was allowed to vary (i.e. Fig. 10). Furthermore, there is a strong positive correlation between the percentage increase in pPv and the number of fitting models.

According to our mineral physics data, transformation of perovskite to post-perovskite always produces an increase in S-wave velocity. Thus, we cannot model our seismic observations with an isothermal backtransition from post-perovskite to perovskite, because for all our seismic data sets, SdS polarity is always positive. We found that it is possible to fit the seismic observations in PdP-positive regions when the pPv to Pv backtransition is accompanied by a temperature change, but in this case we were fitting the data due to thermal effects, because the fitting models contained only small changes in pPv content. It is not possible, with our mineral data set, to fit the seismic observations in PdP-negative regions with a pPv to Pv back-transition accompanied by a temperature change.

In Section 4, generation of reflections using MORB were computed assuming there was no post-perovskite in the system. Recent mineral physics experiments have suggested that if post-perovskite is present in the deep mantle, it may be restricted to, or only produce a sharp phase boundary in, certain chemical compositions, such as MORB and harzburgite (Grocholski *et al.* 2012). In light of these results, we ran a further simulation in which the basalt content changes across the D'' discontinuity (as described in Section 4), but this time all the perovskite within the MORB component (CM) is converted to post-perovskite. In this instance, the fit of PdP-negative regions is enhanced relative to pPv-free MORB (Figs A2 and A3), due to the favourable seismic properties of post-perovskite. The fit of PdP-positive regions is reduced, with the signature of fitting models being dominated once more by a large decrease in temperature. However, the number of fitting models in PdP-positive regions is still typically an order of magnitude greater than in PdP-negative regions. In the Bering Sea, the combined seismic signature of temperature changes and pPv changes mean that the combined polarity and amplitude observations actually favour a decrease in MORB content across the discontinuity rather than an increase.

6 REFLECTIONS FROM OTHER (THERMO)CHEMICAL HETEROGENEITY

We consider briefly the possibility that D'' reflections may be generated by some sort of thermochemical heterogeneity other than those encapsulated by MORB or post-perovskite variations. Changes in the volume of $(\text{Mg}, \text{Fe})\text{SiO}_3$ perovskite relative to $(\text{Mg}, \text{Fe})\text{O}$ are already represented by the simulations involving changes in MORB content (bearing in mind that the seismic properties of MORB depend also on their Fe content, Fig. 8). CaSiO_3 , Al_2O_3 and SiO_2 phases comprise volumetrically minor components of the lower mantle, so we expect that their seismic signature would be secondary relative to the effects of Fe- and Mg-bearing minerals. Furthermore our mineral physics data suggest that Al_2O_3 and free SiO_2 are seismically similar to (Mg,Fe)-perovskite, although CaSiO_3 may be seismically distinct. As a remaining possibility, we test the fit of models in which the iron content changes across the D'' discontinuity, together with a change in temperature (Fig. A4). Models which fit the seismic data do not necessarily correspond directly to something physically meaningful, but illustrate the well-known negative correlation between temperature and iron changes (e.g. Deschamps & Trampert 2003; Cobden *et al.* 2012). PdP-positive

regions are characterized by a decrease in Fe below the discontinuity, whereas PdP-negative regions favour Fe-enriched compositions below the discontinuity; as a secondary effect all regions tend to prefer a decrease in temperature. More models fit in the PdP-positive, SdS-positive regions than the PdP-negative, SdS-positive regions because P-wave velocities are positively correlated with S-wave velocities for both Fe changes and temperature changes. Finally, we test the effect of changing both Fe and Pv content simultaneously (Fig. A5), since geodynamic modelling has suggested that large, low-shear wave velocity provinces (LLSVPs) imaged by seismic tomography may be explained by material enriched in both Fe and Pv (Deschamps *et al.* 2012). Our data from the Pacific in particular sample one of these LLSVPs. We find that in all regions it is possible to generate models, which fit the seismic data by changing both Fe and Pv simultaneously, but no region shows a strong preference for a simultaneous enrichment of Fe and Pv below the discontinuity, due to trade-offs between the seismic effects of temperature, Fe and Pv. This is an indication that what we see at long-wavelengths (a few thousand km) in tomography is difficult to correlate with the finer-scale structures (few hundred kilometres) detected by array seismology—hardly surprising since thermochemical heterogeneity likely occurs at multiple length scales in the deep mantle.

7 DISCUSSION

7.1 Mineral physics uncertainties

Convergence towards a consensus on the depth and sharpness of the Pv–pPv phase boundary will provide an important constraint for further distinguishing between different physical causes of D'' reflections. Likewise, we have imposed only a simple Fe–Mg partitioning, K , between perovskite and magnesiowustite in our modelling (based on experimental constraints placing K between ~ 0.1 and 0.6, e.g. Frost & Langenhorst 2002; McCammon *et al.* 2004; Auzende *et al.* 2008; Sinmyo *et al.* 2008; Sakai *et al.* 2009; Nakajima *et al.* 2012), when in reality, a complex three-way partitioning between perovskite, magnesiowustite and post-perovskite is expected (e.g. Andrault *et al.* 2010). This effect, still poorly constrained, will likely restrict the compositional ranges of Pv, Mw and pPv at D'' depths to be smaller than those used in this study.

Our interpretation relies heavily on the seismic properties predicted by the mineral physics data set. We have incorporated uncertainties in mineral elastic parameters into our modelling by using the uncertainty bounds given in Stixrude & Lithgow-Bertelloni (2011). These bounds are probably an underestimate of the full uncertainties, as forthcoming experimental data will highlight systematic errors in previous data, or discover unanticipated mineral phenomena. However, the compilation of Stixrude & Lithgow-Bertelloni (2011) is the most comprehensive mineral database published to date, and is based upon experimental observations as recent as 2010, thus can be regarded as the most robust, self-consistent data set publicly available.

Future experiments on the minor mantle minerals, that is, Ca- and Al-bearing phases plus free SiO_2 will allow us to constrain the seismic velocities of mineral assemblages more accurately. For example, MORB has a significantly larger CaSiO_3 (Ca–Pv) component than pyrolite or harzburgite (compare Tables 2 and 3), and recent experimental studies have indicated that the seismic velocities of Ca–Pv could be significantly lower than those predicted by our data, if the Ca–Pv is present as a tetragonal rather than cubic

structure (Kudo *et al.* 2012). In this case, it may be more difficult to generate *PdP*-positive, *SdS*-positive reflections via MORB.

While most experiments indicate that the perovskite to post-perovskite transition should be accompanied by a large increase in *S*-wave speed and a smaller change in *P*-wave speed (Oganov & Ono 2004; e.g. Tsuchiya *et al.* 2004; Wookey *et al.* 2005; Wentzcovitch *et al.* 2006), one group has documented only a small (≤ 0.5 per cent) increase in *S*-wave speed (Murakami *et al.* 2007). If the latter is correct, it would likely reduce the compatibility between models and the seismic observations for those regions, which are currently best fit by a *Pv*-*pPv* phase change. This would in turn require an increased contribution from thermochemical heterogeneity or anisotropy to explain the seismic observations.

7.2 Seismic uncertainties

In this study, synthetic waveform amplitudes were computed using a 1-D (full waveform) reflectivity code (Müller 1985; for examples of amplitude modelling, the reader is referred to Weber 1993; Kito *et al.* 2007; Chaloner *et al.* 2009), and we assumed that the observed amplitudes in the seismic data represented the magnitude of the velocity jump across the discontinuity. In reality, complex lateral topography on the D'' reflector can cause focusing and defocusing of seismic energy, which in turn can significantly alter waveform amplitudes (Thomas & Weber 1997). For this reason we place greater confidence on our polarity measurements than our amplitude measurements. However, synthetic modelling indicates that even with the large uncertainty regarding the cause of waveform amplitudes, velocity increases of at least 1 per cent are required to produce detectable *PdP* and *SdS* phases (Weber 1993; Kito *et al.* 2007; Chaloner *et al.* 2009), and we have shown that this is large enough to distinguish between different mineralogical and thermochemical structures (Figs 7 and 10). In order to understand the effects of D'' topography fully, 3-D waveform modelling at the high frequencies of *PdP* and *SdS* phases (which are typically imaged at periods of 0.5–10 s and 3–50 s, respectively) is required, but is currently too computationally expensive. 2.5-D waveform computations are currently in progress (Hempel *et al.*, in preparation) and will provide important insights into the extent to which we can interpret amplitude measurements.

7.3 Observational biases

In our data compilation, we observe both positive and negative polarity *PdP* phases, but the *SdS* phase always shows a positive polarity. The exclusively positive polarity of the *SdS* phase could be an inherent property of the D'' reflector structure, but it is also possible that negative polarity *SdS* phases (i.e. decreases in *S*-velocity across the D'' discontinuity) exist in the Earth but are below the detection threshold of our data analysis. Synthetic models by Gaherty & Lay (1992) and Flores & Lay (2005) have shown that negative velocity changes produce weaker amplitude reflections and may thus be more difficult to observe than positive velocity changes. We calculated the reflection coefficient for *P* and *S* waves as a function of epicentral distance, for both positive and negative velocity contrasts at 2605 km depth (see Fig. B1). We found that the reflection coefficient for *PdP* depends not only on the change in *P*-velocity but also strongly on the concurrent change in *S*-velocity. Where the change in *P* and *S* velocity are of opposite sign, the *P* reflection coefficient is larger at pre-critical distances than for the case where *P* and *S* velocity changes have the same sign. This makes it easier to detect

negative polarity *PdP* waves when the *SdS* has a positive polarity than when it has a negative polarity, and also than when both *PdP* and *SdS* have a positive polarity. In contrast, the magnitude of the reflection coefficient of the *SdS* phase is not influenced by the sign (+ or -) of the *P* velocity change. This means that at most epicentral distances the reflection coefficient of a negative polarity *SdS* is smaller than that of a positive polarity *SdS*, although for a narrow interval of pre-critical distances it has a larger amplitude. Therefore, it should be more difficult, although not necessarily impossible, to detect negative polarity *SdS* phases than positive ones. Thus when attempting to interpret our data in terms of underlying physical structure (Section 7.4) one should bear in mind that our data are likely biased towards detection of positive polarity *SdS* phases.

7.4 Interpretation

In the Caribbean and Southeast Asia, where *PdP* shows a negative polarity and *SdS* a positive polarity, a phase change from perovskite to post-perovskite provides the best fit to the seismic data, out of the different physical models which we tested. The larger amplitude reflections seen in the Caribbean are fit by models containing a higher volume percentage of post-perovskite than those of Southeast Asia, and furthermore Southeast Asia shows a smaller misfit to D'' reflections generated by subducted MORB than the Caribbean does. Our results are thus compatible with the preferred interpretation of Chaloner *et al.* (2009) that D'' reflections under Southeast Asia are produced by a post-perovskite phase transition in combination with a cold slab (based on the local plate tectonic history and thermodynamic arguments). He & Wen (2011) arrived at a similar conclusion, based on combining waveform modelling of D'' reflections with a local tomography model.

A consistency between observations of D'' reflections in the Caribbean and a phase transition from *Pv* to *pPv* has been documented many times (e.g. Hutzko *et al.* 2006, 2008, 2009; Kito *et al.* 2007; Lay 2008); this study takes a step further by testing the post-perovskite hypothesis in a multi-mineralic system and comparatively against other hypotheses.

In Siberia, the Bering Sea and the central Pacific, where *PdP* and *SdS* both show a positive polarity, the probability of fitting the seismic observations via a phase change from perovskite to isotropic post-perovskite is very small, because this phase change does not produce the required > 1 per cent increase in *P*-wave velocity (Fig. 12). If the temperature is allowed to vary in our simulations, the seismic properties of *PdP* and *SdS* are most frequently fit by models in which a large (~ 500 –1000 K) temperature drop occurs across D'' , regardless of whether the accompanying chemical changes involve post-perovskite or MORB. If temperature is kept fixed, or only small *T* variations are allowed, then the D'' reflections in these regions can readily be explained by changes in MORB content (usually an increase, unless the MORB is particularly iron-rich or post-perovskite-rich). Theoretically, it is possible to explain D'' reflections in *PdP*-positive, *SdS*-positive regions purely with thermal effects, if one considers only the seismic velocity changes required. However, we prefer an interpretation in which chemical or mineralogical changes are dominant over thermal effects, because D'' reflections are detected at high frequencies (0.5–10 s) in the *P*-wave data, indicating that the vertical thickness of the reflecting zone should be less than ~ 90 km (Weber *et al.* 1996), and possibly as narrow as 8–30 km (Wysession *et al.* 1998; Lay 2008). It is difficult geodynamically to sustain negative thermal anomalies with an amplitude of several hundred degrees over wavelengths of a few 10 s

of kilometres (e.g. Ricard *et al.* 2005). Although subducting slabs can retain a significant negative temperature anomaly (>500 K) as far as the CMB (Tan *et al.* 2002), the largest amplitude anomaly will be at the centre of the slab. In this study, we have modelled D'' reflections with MORB, which would be at the edge of a subducting slab. Because the thickness of (undeformed) MORB is ~7 km, a thermal anomaly of 500° would be lost within 2 Myr (Kaneshima & Helffrich 1999), that is, long before reaching the D'' region.

The regions underneath Siberia and the Bering Sea are both sites of former or ongoing subduction (Lithgow-Bertelloni & Richards 1998), and it is therefore plausible to attribute PdP and SdS observations to reflections from subducted MORB in these locations. This explanation is in addition to the possibility that the reflections are generated by anisotropy in post-perovskite (Thomas *et al.* 2011). Chemical heterogeneity not related to subduction (e.g. iron depletion under the Bering Sea) could likewise produce D'' reflections (Figs A4 and A5), although we must search for a physical cause for such heterogeneity. We note further that because the data for the Bering Sea show weaker signals than for the other regions (e.g. see Figs 3–5) with less certain PdP and SdS polarities, these data should not be subjected to over-interpretation, and the cause of D'' reflections remains more speculative here than in the other four regions.

The Caribbean is also a region of active subduction. Geodynamic reconstructions indicate that subduction of the Farallon Plate beneath the Caribbean could reach the CMB (Lithgow-Bertelloni & Richards 1998), while seismic tomography models (Grand *et al.* 1997; Grand 2002) have been interpreted as showing a slab which appears to buckle and fold above the CMB (Hutko *et al.* 2006). D'' reflections in the Caribbean have therefore not only been interpreted as due to a phase transition from perovskite to post-perovskite, but also could come from subducted material (Thomas *et al.* 2004a), or a combination of phase transition plus subducted material (Hutko *et al.* 2006). One possible interpretation of our results is therefore as illustrated in Fig. 13, in which a slab travels undeformed towards the CMB in Siberia, and D'' reflections are generated from the MORB on the topside of the slab, while the Caribbean, the slab folds back on itself and D'' reflections are generated by post-perovskite in the non-MORB underside of the slab.

The Pacific is interesting, because the average seismic properties of the D'' reflections are identical to Siberia, but it is not a site of recent or active subduction. If MORB material is indeed present and causing D'' reflections (as is compatible with our seismic observations), it may have been swept aside from surrounding regions by convection (e.g. McNamara & Zhong 2005). At the wavelength of seismic tomography (thousands of kilometres), these reflections lie within a large region of low S-wave velocity (LLSVP). The apparent

depths of D'' reflectors (100–300 km above the CMB) are mostly greater than the apparent upper boundary of the LLSVP (~500 km above the CMB), so it is likely that we are seeing structures within the interior of the LLSVP. Deschamps *et al.* (2012) inferred from combined seismic and geodynamic modelling that LLSVPs are unlikely to consist of MORB. If correct, this interpretation would imply that any MORB material which generates D'' reflections represents a small component of the total structure within the LLSVP. If, as alternative studies suggest (e.g. Ohta *et al.* 2008), MORB is a major component of the LLSVP, then MORB itself would not be seismically distinct to generate reflections without significant internal layering in the LLSVP.

Our seismic data for the Pacific are noteworthy for displaying strong amplitude PdP and SdS phases, from which we inferred larger velocity increases than in previous studies. We estimated velocity increases of 1–3 and 2–3 per cent for P and S waves, respectively, compared with 0.5–1.5 per cent for P and 0.5–2.3 per cent for S in previous studies (Reasoner & Revenaugh 1999; Russell *et al.* 2001; Avants *et al.* 2006; Lay *et al.* 2006; Hutko *et al.* 2009). Previous studies of the Pacific have attributed D'' reflections to a lens of post-perovskite surrounded by perovskite (Avants *et al.* 2006; Lay *et al.* 2006; Hutko *et al.* 2009). Detailed mineral physics modelling in this study indicates that isotropic post-perovskite is unlikely to generate D'' reflections in this region, due to the large amplitude PdP phase. However, as with all other study regions, anisotropy in post-perovskite is a viable alternative mechanism for generating D'' reflections, which could mitigate apparent inconsistency between different studies of the region.

7.5 Summary and conclusions

We have shown that by combining seismic observations with mineral physics data, and taking uncertainties in mantle mineralogy and mineral elastic parameters into account, it is possible to explain the polarities and amplitudes of PdP and SdS arrivals using many different thermochemical models. Although we cannot attribute a unique cause to the seismic observations in each geographic region, we can observe statistically significant differences between the different regions in terms of which thermochemical structures fit best. Additionally, polarities alone can be used to discriminate between different possibilities, without the use of amplitude measurements, although of course amplitudes provide additional constraints. Our study represents a preliminary, but systematic, interpretation of D'' reflections, to be built upon as more mineral physics data, more geographic coverage of the lowermost mantle, and a better understanding of 3-D wave-propagation at high frequencies, are acquired.

Our study illustrates that the D'' discontinuity does not have to have a single global cause, and may be generated by different physical structures in different regions. Applying Occam's razor, a unifying cause of D'' reflections would be preferred, and this may be achieved via anisotropy in post-perovskite. Anisotropy should thus be an area on which to concentrate future efforts. In particular, computation of seismic anisotropy for multi-mineral assemblages and in minerals other than post-perovskite, that is, magnesiowustite (Yamazaki & Karato 2002), will be required. Seismically, observational constraints on anisotropy can come from crossing ray-paths sampling the same region of D'', and SKS-splitting studies.

Underneath Siberia and the Bering Sea, we find that the seismic properties of PdP and SdS phases are readily explained by the presence of subducted MORB, compatible with the regions' subduction histories, but that it is difficult to model the data with a phase change

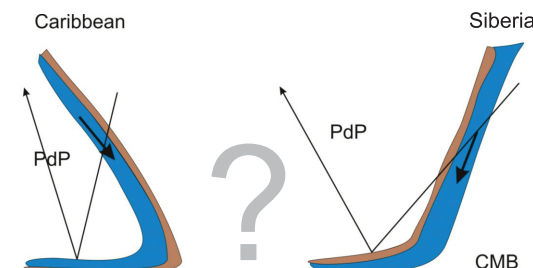


Figure 13. Speculative cartoon showing one possible mechanism for generating the different properties of D'' reflections underneath the Caribbean compared with Siberia. Brown represents MORB crust and blue is the underlying harzburgitic lithosphere.

from perovskite to isotropic post-perovskite. The seismic properties of PdP and SdS phases in the Pacific are the same as for Siberia, but the former is not a direct site of recent subduction. This indicates that either subducted material has been convectively transported and accumulated from elsewhere, or anisotropy plays a role in generating the D'' reflections. Beneath the Caribbean and Southeast Asia, the seismic properties of PdP and SdS phases are difficult to model when no post-perovskite is present, that is, through subduction alone, but can easily be modelled when a phase change from perovskite to (isotropic) post-perovskite occurs. Thus, the D'' reflections in these regions may arise from the presence of post-perovskite alone or post-perovskite in conjunction with the presence of a slab.

It is important to bear in mind that while certain aspects of the seismic properties of MORB or post-perovskite are not currently well-constrained (Section 7.2), and may ultimately lead to a different interpretation than the one presented here, we have shown that within the (large) uncertainty bounds applied in this study, it is currently straightforward to fit the seismic properties of D'' reflections in certain geographic locations using MORB, with or without a concurrent temperature anomaly. This possibility has been somewhat discounted in recent years in favour of post-perovskite, and deserves further attention.

ACKNOWLEDGEMENTS

Fig. 2 was produced using the program GMT (Wessel & Smith 1995) and seismic data were processed using the software SeismicHandler (Stammler 1993). The authors thank two anonymous reviewers for helpful comments, which improved the manuscript significantly. This work was funded by the DFG (German Research Foundation) on Grant number TH1530/5-1.

REFERENCES

- Akber-Knutson, S. & Bukowinski, M., 2004. The energetics of aluminum solubility into $MgSiCO(3)$ perovskite at lower mantle conditions, *Earth planet. Sci. Lett.*, **220**, 317–330.
- Ammann, M.W., Brodholt, J.P., Wookey, J. & Dobson, D.P., 2010. First-principles constraints on diffusion in lower-mantle minerals and a weak D'' layer, *Nature*, **465**, 462–465.
- Andrault, D., Munoz, M., Bolfan-Casanova, N., Guignot, N., Perrillat, J., Aquilanti, G. & Pascarelli, S., 2010. Experimental evidence for perovskite and post-perovskite coexistence throughout the whole D'' region, *Earth planet. Sci. Lett.*, **293**, 90–96.
- Auzende, A., Badro, J., Ryerson, F.J., Weber, P.K., Fallon, S.J., Addad, A., Siebert, J. & Fiquet, G., 2008. Element partitioning between magnesium silicate perovskite and ferropericlase: New insights into bulk lower-mantle geochemistry, *Earth planet. Sci. Lett.*, **269**, 164–174.
- Avants, M., Lay, T., Russell, S. & Garnero, E., 2006. Shear velocity variation within the D'' region beneath the central Pacific, *J. geophys. Res.-Solid Earth*, **111**, B05305, doi:10.1029/2004JB003270.
- Brodholt, J.P., Helffrich, G. & Trampert, J., 2007. Chemical versus thermal heterogeneity in the lower mantle: the most likely role of anelasticity, *Earth planet. Sci. Lett.*, **262**, 429–437.
- Bullen, K.E., 1949. Compressibility-pressure hypothesis and the Earth's interior, *Geophys. J. Int.*, **5**, 335–368.
- Cammarano, F., Goes, S., Deuss, A. & Giardini, D., 2005. Is a pyrolytic adiabatic mantle compatible with seismic data? *Earth planet. Sci. Lett.*, **232**, 227–243.
- Caracas, R. & Cohen, R., 2005. Prediction of a new phase transition in Al_2O_3 at high pressures, *Geophys. Res. Lett.*, **32**, L06303, doi:10.1029/2004GL022204.
- Catalli, K., Shim, S. & Prakapenka, V., 2009. Thickness and Clapeyron slope of the post-perovskite boundary, *Nature*, **462**, 782–785.
- Chaloner, J.W., Thomas, C. & Rietbrock, A., 2009. P- and S-wave reflectors in D'' beneath southeast Asia, *Geophys. J. Int.*, **179**, 1080–1092.
- Chambers, K. & Woodhouse, J.H., 2006. Transient D'' discontinuity revealed by seismic migration, *Geophys. Res. Lett.*, **33**, L17312, doi:10.1029/2006GL027043.
- Christensen, U.R., 1989. Models of mantle convection—one or several layers, *Phil. Trans. R. Soc. Lond., A-Math. Phys. Eng. Sci.*, **328**, 417–424.
- Christensen, U.R. & Hofmann, A.W., 1994. Segregation of subducted oceanic-crust in the convecting mantle, *J. geophys. Res. Solid Earth*, **99**, 19 867–19 884.
- Cobden, L., Goes, S., Cammarano, F. & Connolly, J.A.D., 2008. Thermochemical interpretation of one-dimensional seismic reference models for the upper mantle: evidence for bias due to heterogeneity, *Geophys. J. Int.*, **175**, 627–648.
- Cobden, L., Goes, S., Ravenna, M., Styles, E., Cammarano, F., Gallagher, K. & Connolly, J.A.D., 2009. Thermochemical interpretation of 1-D seismic data for the lower mantle: the significance of nonadiabatic thermal gradients and compositional heterogeneity, *J. geophys. Res.-Solid Earth*, **114**, B11309, doi:10.1029/2008JB006262.
- Cobden, L., Mosca, I., Trampert, J. & Ritsema, J., 2012. On the likelihood of post-perovskite near the core-mantle boundary: a statistical interpretation of seismic observations, *Phys. Earth planet. Inter.*, **210–211**, 21–35.
- Davies, D., Kelly, E. & Filson, J., 1971. Vespa process for analysis of seismic signals, *Nat. Phys. Sci.*, **232**, 8–13.
- Deschamps, F. & Trampert, J., 2003. Mantle tomography and its relation to temperature and composition, *Phys. Earth planet. Inter.*, **140**, 277–291.
- Deschamps, F., Cobden, L. & Tackley, P.J., 2012. The primitive nature of large low shear wave velocity provinces, *Earth planet. Sci. Lett.*, **349–350**, 198–208.
- Flores, C. & Lay, T., 2005. The trouble with seeing double, *Geophys. Res. Lett.*, **32**, L24305, doi:10.1029/2005GL024366.
- Frost, D. & Langenhorst, F., 2002. The effect of Al_2O_3 on Fe-Mg partitioning between magnesiowustite and magnesium silicate perovskite, *Earth planet. Sci. Lett.*, **199**, 227–241.
- Gaherty, J.B. & Lay, T., 1992. Investigation of laterally heterogeneous shear velocity structure in D'' beneath Eurasia, *J. geophys. Res.-Solid Earth*, **97**, 417–435.
- Grand, S., 2002. Mantle shear-wave tomography and the fate of subducted slabs, *Phil. Trans. R. Soc. Lond., A-Math. Phys. Eng. Sci.*, **360**, 2475–2491.
- Grand, S., van der Hilst, R.D. & Widjiantoro, S., 1997. Global seismic tomography: a snapshot of convection in the Earth, *GSA Today*, **7**, 1–7.
- Grocholski, B., Catalli, K., Shim, S. & Prakapenka, V., 2012. Mineralogical effects on the detectability of the postperovskite boundary, *Proc. Natl. Acad. Sci. USA*, **109**, 2275–2279.
- He, Y. & Wen, L., 2011. Seismic velocity structures and detailed features of the D'' discontinuity near the core-mantle boundary beneath eastern Eurasia, *Phys. Earth planet. Inter.*, **189**, 176–184.
- Hernlund, J.W., Thomas, C. & Tackley, P.J., 2005. A doubling of the post-perovskite phase boundary and structure of the Earth's lowermost mantle, *Nature*, **434**, 882–886.
- Hirose, K., 2007. Discovery of post-perovskite phase transition and the nature of D'' layer, in *Post-Perovskite: The Last Mantle Phase Transition*, pp. 19–35, eds Hirose, K., Brodholt, J., Lay, T. & Yuen, D.A., American Geophysical Union, Washington, DC.
- Hirose, K., Takafuji, N., Sata, N. & Ohishi, Y., 2005. Phase transition and density of subducted MORB crust in the lower mantle, *Earth planet. Sci. Lett.*, **237**, 239–251.
- Hirose, K., Takafuji, N., Fujino, K., Shieh, S.R. & Duffy, T.S., 2008. Iron partitioning between perovskite and post-perovskite: a transmission electron microscope study, *Am. Mineral.*, **93**, 1678–1681.
- Hofmann, A., 1988. Chemical differentiation of the Earth—the relationship between mantle, continental-crust, and oceanic-crust, *Earth planet. Sci. Lett.*, **90**, 297–314.
- Hunt, S.A., Weidner, D.J., Li, L., Wang, L., Walte, N.P., Brodholt, J.P. & Dobson, D.P., 2009. Weakening of calcium iridate during its transformation from perovskite to post-perovskite, *Nat. Geosci.*, **2**, 794–797.

- Hutko, A., Lay, T., Garnero, E. & Revenaugh, J., 2006. Seismic detection of folded, subducted lithosphere at the core-mantle boundary, *Nature*, **441**, 333–336.
- Hutko, A.R., Lay, T., Revenaugh, J. & Garnero, E.J., 2008. Anticorrelated seismic velocity anomalies from post-perovskite in the lowermost mantle, *Science*, **320**, 1070–1074.
- Hutko, A.R., Lay, T. & Revenaugh, J., 2009. Localized double-array stacking analysis of Pcp: D'' and ULVZ structure beneath the Cocos plate, Mexico, central Pacific, and north Pacific, *Phys. Earth planet. Inter.*, **173**, 60–74.
- Irifune, T. & Ringwood, A., 1993. Phase-transformations in subducted oceanic-crust and buoyancy relationships at depths of 600–800 km in the mantle, *Earth planet. Sci. Lett.*, **117**, 101–110.
- Kaneshima, S. & Helffrich, G., 1998. Detection of lower mantle scatterers northeast of the Marianna subduction zone using short-period array data, *J. geophys. Res.-Solid Earth*, **103**, 4825–4838.
- Kaneshima, S. & Helffrich, G., 1999. Dipping low-velocity layer in the mid-lower mantle: evidence for geochemical heterogeneity, *Science*, **283**, 1888–1891.
- Karason, H. & van der Hilst, R., 2001. Tomographic imaging of the lower-most mantle with differential times of refracted and diffracted core phases (PKP, P-diff), *J. geophys. Res.-Solid Earth*, **106**, 6569–6587.
- Kawai, K. & Geller, R.J., 2010. Waveform inversion for localized seismic structure and an application to D'' structure beneath the Pacific, *J. geophys. Res.-Solid Earth*, **115**, B01305, doi:10.1029/2009JB006503.
- Kendall, J. & Nangini, C., 1996. Lateral variations in D'' below the Caribbean, *Geophys. Res. Lett.*, **23**, 399–402.
- Kennett, B., Engdahl, E. & Buland, R., 1995. Constraints on seismic velocities in the earth from travel-times, *Geophys. J. Int.*, **122**, 108–124.
- Kito, T., Rost, S., Thomas, C. & Garnero, E.J., 2007. New insights into the P- and S-wave velocity structure of the D'' discontinuity beneath the Cocos plate, *Geophys. J. Int.*, **169**, 631–645.
- Knittle, E. & Jeanloz, R., 1989. Simulating the core-mantle boundary—an experimental-study of high-pressure reactions between silicates and liquid-iron, *Geophys. Res. Lett.*, **16**, 609–612.
- Kudo, Y., Hirose, K., Murakami, M., Asahara, Y., Ozawa, H., Ohishi, Y. & Hirao, N., 2012. Sound velocity measurements of CaSiO₃ perovskite to 133 GPa and implications for lowermost mantle seismic anomalies, *Earth planet. Sci. Lett.*, **349–350**, 1–7.
- Lay, T., 2008. Sharpness of the D'' discontinuity beneath the Cocos Plate: implications for the perovskite to post-perovskite phase transition, *Geophys. Res. Lett.*, **35**, L03304, doi:10.1029/2007GL032465.
- Lay, T. & Helmberger, D., 1983. A lower mantle S-wave tripllication and the shear velocity structure of D'', *Geophys. J. R. astr. Soc.*, **75**, 799–837.
- Lay, T., Garnero, E. & Russell, S., 2004. Lateral variation of the D'' discontinuity beneath the Cocos Plate, *Geophys. Res. Lett.*, **31**, L15612, doi:10.1029/2004GL020300.
- Lay, T., Hernlund, J., Garnero, E.J. & Thorne, M.S., 2006. A post-perovskite lens and D'' heat flux beneath the central Pacific, *Science*, **314**, 1272–1276.
- Lithgow-Bertelloni, C. & Richards, M., 1998. The dynamics of Cenozoic and Mesozoic plate motions, *Rev. Geophys.*, **36**, 27–78.
- Liu, X., Tromp, J. & Dziewonski, A., 1998. Is there a first-order discontinuity in the lowermost mantle? *Earth planet. Sci. Lett.*, **160**, 343–351.
- Mao, W. *et al.*, 2004. Ferromagnesian postperovskite silicates in the D'' layer of the Earth, *Proc. Natl. Acad. Sci. USA*, **101**, 15 867–15 869.
- McCammon, C., Lauterbach, S., Seifert, F., Langenhorst, F. & van Aken, P., 2004. Iron oxidation state in lower mantle mineral assemblages. Part I. Empirical relations derived from high-pressure experiments, *Earth planet. Sci. Lett.*, **222**, 435–449.
- McNamara, A.K. & Zhong, S.J., 2005. Thermochemical structures beneath Africa and the Pacific Ocean, *Nature*, **437**, 1136–1139.
- Mosca, I., Cobden, L., Deuss, A., Ritsema, J. & Trampert, J., 2012. Seismic and mineralogical structures of the lower mantle from probabilistic tomography, *J. geophys. Res.-Solid Earth*, **117**, B06304, doi:10.1029/2011JB008851.
- Muirhead, K. & Datt, R., 1976. N-th root process applied to seismic array data, *Geophys. J. R. astr. Soc.*, **47**, 197–210.
- Müller, G., 1985. The reflectivity method—a tutorial, *J. Geophys.*, **58**, 153–174.
- Murakami, M., Hirose, K., Ono, S. & Ohishi, Y., 2003. Stability of CaCl₂-type and alpha-PbO₂-type SiO₂ at high pressure and temperature determined by in-situ X-ray measurements, *Geophys. Res. Lett.*, **30**, 1207, doi:10.1029/2002GL016722.
- Murakami, M., Ohishi, Y., Hirao, N. & Hirose, K., 2012. A perovskitic lower mantle inferred from high-pressure, high-temperature sound velocity data, *Nature*, **485**, 90–94.
- Murakami, M., Hirose, K., Kawamura, K., Sata, N. & Ohishi, Y., 2004. Post-perovskite phase transition in MgSiO₃, *Science*, **304**, 855–858.
- Murakami, M., Sinogeikin, S.V., Bass, J.D., Sata, N., Ohishi, Y. & Hirose, K., 2007. Sound velocity of MgSiO₃ post-perovskite phase: a constraint on the D'' discontinuity, *Earth planet. Sci. Lett.*, **259**, 18–23.
- Nakagawa, T. & Tackley, P., 2004. Thermo-chemical structure in the mantle arising from a three-component convective system and implications for geochemistry, *Phys. Earth planet. Inter.*, **146**, 125–138.
- Nakajima, Y., Frost, D.J. & Rubie, D.C., 2012. Ferrous iron partitioning between magnesium silicate perovskite and ferropericlase and the composition of perovskite in the Earth's lower mantle, *J. geophys. Res.-Solid Earth*, **117**, B08201, doi:10.1029/2012JB009151.
- Oganov, A.R. & Ono, S., 2004. Theoretical and experimental evidence for a post-perovskite phase of MgSiO₃ in Earth's D'' layer, *Nature*, **430**, 445–448.
- Oganov, A. & Ono, S., 2005. The high-pressure phase of alumina and implications for Earth's D'' layer, *Proc. Natl. Acad. Sci. USA*, **102**, 10 828–10 831.
- Ohta, K., Hirose, K., Lay, T., Sata, N. & Ohishi, Y., 2008. Phase transitions in pyrolite and MORB at lowermost mantle conditions: implications for a MORB-rich pile above the core-mantle boundary, *Earth planet. Sci. Lett.*, **267**, 107–117.
- Ono, S., Ito, E. & Katsura, T., 2001. Mineralogy of subducted basaltic crust (MORB) from 25 to 37 GPa, and chemical heterogeneity of the lower mantle, *Earth planet. Sci. Lett.*, **190**, 57–63.
- Ono, S., Ohishi, Y., Isshiki, M. & Watanuki, T., 2005. In situ X-ray observations of phase assemblages in peridotite and basalt compositions at lower mantle conditions: implications for density of subducted oceanic plate, *J. geophys. Res.-Solid Earth*, **110**, B02208, doi:10.1029/2004JB003196.
- Perrillat, J., Ricolleau, A., Daniel, I., Fiquet, G., Mezouar, M., Guignot, N. & Cardon, H., 2006. Phase transformations of subducted basaltic crust in the upmost lower mantle, *Phys. Earth planet. Inter.*, **157**, 139–149.
- Reasoner, C. & Revenaugh, J., 1999. Short-period P wave constraints on D'' reflectivity, *J. geophys. Res.-Solid Earth*, **104**, 955–961.
- Ricard, Y., Mattern, E. & Matas, J., 2005. Synthetic tomographic images of slabs from mineral physics, in *Earth's Deep Mantle: Structure, Composition and Evolution*, pp. 285–302, eds van der Hilst, R.D., Bass, J.D., Matas, J. & Trampert, J., American Geophysical Union, Washington, DC.
- Ricolleau, A. *et al.*, 2010. Phase relations and equation of state of a natural MORB: implications for the density profile of subducted oceanic crust in the Earth's lower mantle RID A-3366–2008, *J. geophys. Res.-Solid Earth*, **115**, B08202, doi:10.1029/2009JB006709.
- Ritsema, J., Deuss, A., van Heijst, H.J. & Woodhouse, J.H., 2011. S40RTS: a degree-40 shear-velocity model for the mantle from new Rayleigh wave dispersion, teleseismic traveltimes and normal-mode splitting function measurements, *Geophys. J. Int.*, **184**, 1223–1236.
- Rost, S. & Thomas, C., 2009. Improving seismic resolution through array processing techniques, *Surv. Geophys.*, **30**, 271–299.
- Rost, S. & Thomas, C., 2002. Array seismology: methods and applications, *Rev. Geophys.*, **40**, 1008, doi:10.1029/2000RG000100.
- Russell, S., Reasoner, C., Lay, T. & Revenaugh, J., 2001. Coexisting shear- and compressional-wave seismic velocity discontinuities beneath the central Pacific, *Geophys. Res. Lett.*, **28**, 2281–2284.
- Sakai, T. *et al.*, 2009. Fe-Mg partitioning between perovskite and ferropericlase in the lower mantle, *Am. Mineral.*, **94**, 921–925.
- Scherbaum, F., Kruger, F. & Weber, M., 1997. Double beam imaging: mapping lower mantle heterogeneities using combinations of source and receiver arrays, *J. geophys. Res.-Solid Earth*, **102**, 507–522.

- Schimmel, M. & Paulsen, H., 1997. Noise reduction and detection of weak, coherent signals through phase-weighted stacks, *Geophys. J. Int.*, **130**, 497–505.
- Shieh, S., Duffy, T., Kubo, A., Shen, G., Prakapenka, V., Sata, N., Hirose, K. & Ohishi, Y., 2006. Equation of state of the postperovskite phase synthesized from a natural $(\text{Mg}, \text{Fe})\text{SiO}_3$ orthopyroxene, *Proc. Natl. Acad. Sci. USA*, **103**, 3039–3043.
- Shim, S.H., Duffy, T.S., Jeanloz, R. & Shen, G., 2004. Stability and crystal structure of MgSiO_3 perovskite to the core-mantle boundary, *Geophys. Res. Lett.*, **31**, L10603, doi:10.1029/2004GL019639.
- Sidorin, I., Gurnis, M. & Helmberger, D., 1999a. Dynamics of a phase change at the base of the mantle consistent with seismological observations, *J. geophys. Res.-Solid Earth*, **104**, 15 005–15 023.
- Sidorin, I., Gurnis, M. & Helmberger, D., 1999b. Evidence for a ubiquitous seismic discontinuity at the base of the mantle, *Science*, **286**, 1326–1331.
- Sinmyo, R., Hirose, K., Nishio-Hamane, D., Seto, Y., Fujino, K., Sata, N. & Ohishi, Y., 2008. Partitioning of iron between perovskite/postperovskite and ferropericlase in the lower mantle, *J. geophys. Res.-Solid Earth*, **113**, B11204, doi:10.1029/2008JB005730.
- Stackhouse, S. & Brodholt, J.P., 2007. High-temperature elasticity of MgSiO_3 post-perovskite, in *Post-Perovskite: The Last Mantle Phase Transition*, pp. 99–113, eds Hirose, K., Brodholt, J.P., Lay, T. & Yuen, D., American Geophysical Union, Washington, DC.
- Stammer, K., 1993. Seismicandler programmable multichannel data handler for interactive and automatic processing of seismological analyses, *Comput. Geosci.*, **19**, 135–140.
- Stixrude, L. & Bukowinski, M., 1992. Stability of $(\text{Mg}, \text{Fe})\text{SiO}_3$ perovskite and the structure of the lowermost mantle, *Geophys. Res. Lett.*, **19**, 1057–1060.
- Stixrude, L. & Lithgow-Bertelloni, C., 2011. Thermodynamics of mantle minerals. Part II. Phase equilibria, *Geophys. J. Int.*, **184**, 1180–1213.
- Tan, E., Gurnis, M. & Han, L., 2002. Slabs in the lower mantle and their modulation of plume formation, *Geochem. Geophys. Geosyst.*, **3**, 1067, doi:10.1029/2001GC000238.
- Tateno, S., Hirose, K., Sata, N. & Ohishi, Y., 2005. Phase relations in $\text{Mg}_3\text{Al}_2\text{Si}_3\text{O}_{12}$ to 180 GPa: effect of Al on post-perovskite phase transition, *Geophys. Res. Lett.*, **32**, L15306, doi:10.1029/2005GL023309.
- Tateno, S., Hirose, K., Sata, N. & Ohishi, Y., 2007. Solubility of FeO in $(\text{Mg}, \text{Fe})\text{SiO}_3$ perovskite and the post-perovskite phase transition, *Phys. Earth planet. Inter.*, **160**, 319–325.
- Thomas, C. & Weber, M., 1997. P velocity heterogeneities in the lower mantle determined with the German regional seismic network. Improvement of previous models and results of 2D modelling, *Phys. Earth planet. Inter.*, **101**, 105–117.
- Thomas, C., Kendall, J.-M. & Weber, M., 2002. The lowermost mantle beneath northern Asia? Part I. Multi-azimuth studies of a D'' heterogeneity, *Geophys. J. Int.*, **151**, 279–295.
- Thomas, C., Garnero, E.J. & Lay, T., 2004a. High-resolution imaging of lowermost mantle structure under the Cocos plate, *J. geophys. Res.-Solid Earth*, **109**, B08307, doi:10.1029/2004JB003013.
- Thomas, C., Kendall, J.M. & Lowman, J., 2004b. Lower-mantle seismic discontinuities and the thermal morphology of subducted slabs, *Earth planet. Sci. Lett.*, **225**, 105–113.
- Thomas, C., Wookey, J., Brodholt, J. & Fieseler, T., 2011. Anisotropy as cause for polarity reversals of D'' reflections, *Earth planet. Sci. Lett.*, **307**, 369–376.
- Trampert, J., Vacher, P. & Vlaar, N., 2001. Sensitivities of seismic velocities to temperature, pressure and composition in the lower mantle, *Phys. Earth planet. Inter.*, **124**, 255–267.
- Trampert, J., Deschamps, F., Resovsky, J. & Yuen, D., 2004. Probabilistic tomography maps chemical heterogeneities throughout the lower mantle, *Science*, **306**, 853–856.
- Tsuchiya, J. & Tsuchiya, T., 2008. Postperovskite phase equilibria in the $\text{MgSiO}_3\text{-Al}_2\text{O}_3$ system, *Proc. Natl. Acad. Sci. USA*, **105**, 19 160–19 164.
- Tsuchiya, T., Tsuchiya, J., Umemoto, K. & Wentzcovitch, R., 2004. Phase transition in MgSiO_3 perovskite in the earth's lower mantle, *Earth planet. Sci. Lett.*, **224**, 241–248.
- van der Hilst, R.D., de Hoop, M.V., Wang, P., Shim, S.-H., Ma, P. & Tenorio, L., 2007. Seismostratigraphy and thermal structure of Earth's core-mantle boundary region, *Science*, **315**, 1813–1817.
- Wallace, M. & Thomas, C., 2005. Investigating D'' structure beneath the North Atlantic, *Phys. Earth planet. Inter.*, **151**, 115–127.
- Weber, M., 1993. P-wave and S-wave reflections from anomalies in the lowermost mantle, *Geophys. J. Int.*, **115**, 183–210.
- Weber, M. & Kornig, M., 1990. Lower mantle inhomogeneities inferred from Pcp precursors, *Geophys. Res. Lett.*, **17**, 1993–1996.
- Weber, M. & Wicks, C., 1996. Reflections from a distant subduction zone, *Geophys. Res. Lett.*, **23**, 1453–1456.
- Weber, M., Davis, J.P., Thomas, C., Krüger, F., Scherbaum, F., Schlittenhardt, J. & Körnig, M., 1996. The structure of the lowermost mantle as determined from using seismic arrays, in *Seismic Modelling of the Earth's structure*, pp. 399–442, eds Boschi, E., Ekström, G. & Morelli, A., Instituto Nazionale di Geofisica, Rome.
- Wentzcovitch, R.M., Tsuchiya, T. & Tsuchiya, J., 2006. MgSiO_3 post-perovskite at D'' conditions, *Proc. Natl. Acad. Sci. USA*, **103**, 543–546.
- Wessel, P. & Smith, W.H.F., 1995. New version of the Generic Mapping Tools released, *EOS, Trans. Am. geophys. Un.*, **76**, 329.
- Wookey, J., Stackhouse, S., Kendall, J.M., Brodholt, J. & Price, G.D., 2005. Efficacy of the post-perovskite phase as an explanation for lowermost-mantle seismic properties, *Nature*, **438**, 1004–1007.
- Wysession, M.E., Lay, T., Revenaugh, J., Williams, Q., Garnero, E.J., Jeanloz, R. & Kellogg, L.H., 1998. The D'' discontinuity and its implications, in *The Core-Mantle Boundary Region*, pp. 273–298, eds Gurnis, M., Wysession, M.E., Knittle, E. & Buffet, B.A., American Geophysical Union, Washington, DC.
- Yamazaki, D. & Karato, S., 2002. Fabric development in $(\text{Mg}, \text{Fe})\text{O}$ during large strain, shear deformation: implications for seismic anisotropy in Earth's lower mantle, *Phys. Earth planet. Inter.*, **131**, 251–267.
- Zhang, F. & Oganov, A.R., 2006. Mechanisms of Al^{3+} incorporation in MgSiO_3 post-perovskite at high pressures, *Earth planet. Sci. Lett.*, **248**, 69–76.

APPENDIX A

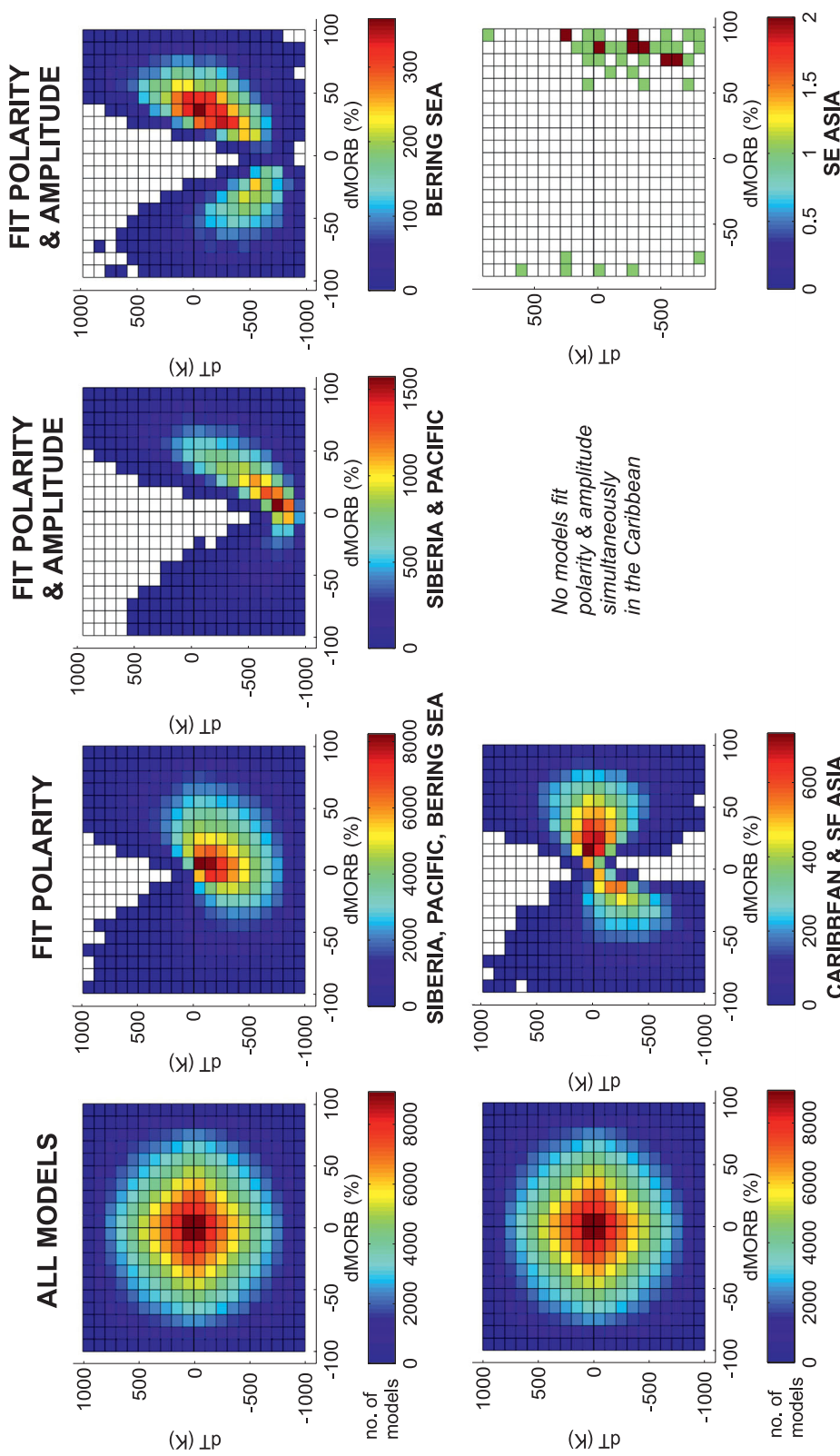


Figure A1. The result of modelling D'' reflections via a change in MORB content and concurrently, smaller amplitude changes in temperature than those allowed in Fig. 7 (i.e. ± 1000 K instead of ± 2000 K). Plotted above are 2-D frequency distributions showing number of models versus change in MORB content and change in temperature from above to below the D'' discontinuity. Left-hand column shows the distribution for 1 million initial models, other columns show the remaining models after fitting waveform polarities and amplitudes in different regions. Changes in MORB content become more important relative to changes in temperature in terms of fitting the seismic observations compared with Fig. 7, and a clear preference for increases in MORB content rather than decreases becomes visible for Siberia, the Pacific and the Bering Sea.

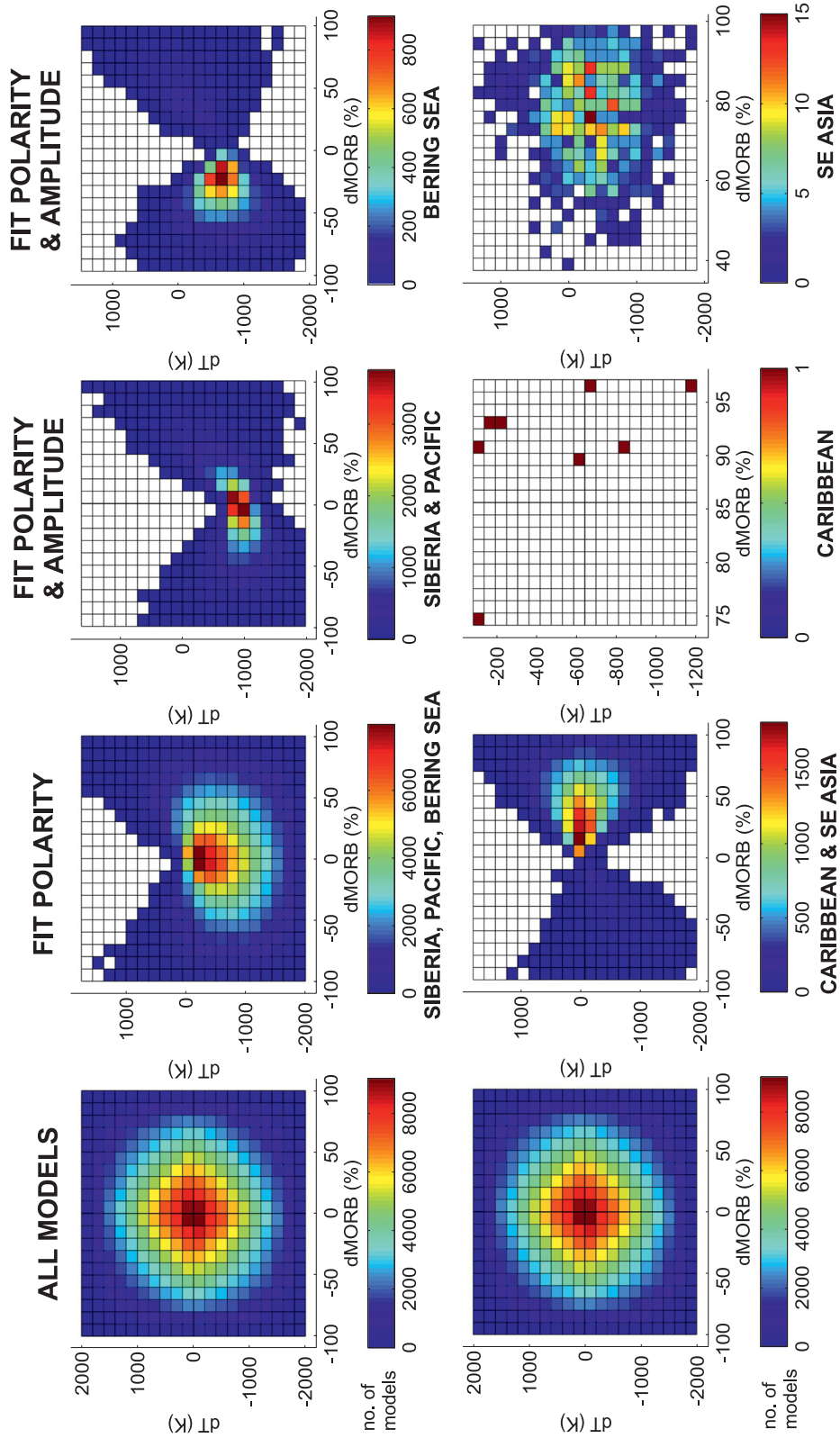


Figure A2. The result of modelling D'' reflections via a change in MORB content and concurrent change in temperature, where all the Mg_2Fe and Al perovskite has converted to post-perovskite within the MORB. Plotted above are 2-D frequency distributions showing number of models versus change in MORB content and change in temperature from above to below the D'' discontinuity. Left-hand column shows the distribution for 1 million initial models, other columns show the remaining models after fitting waveform polarities and amplitudes in different regions.

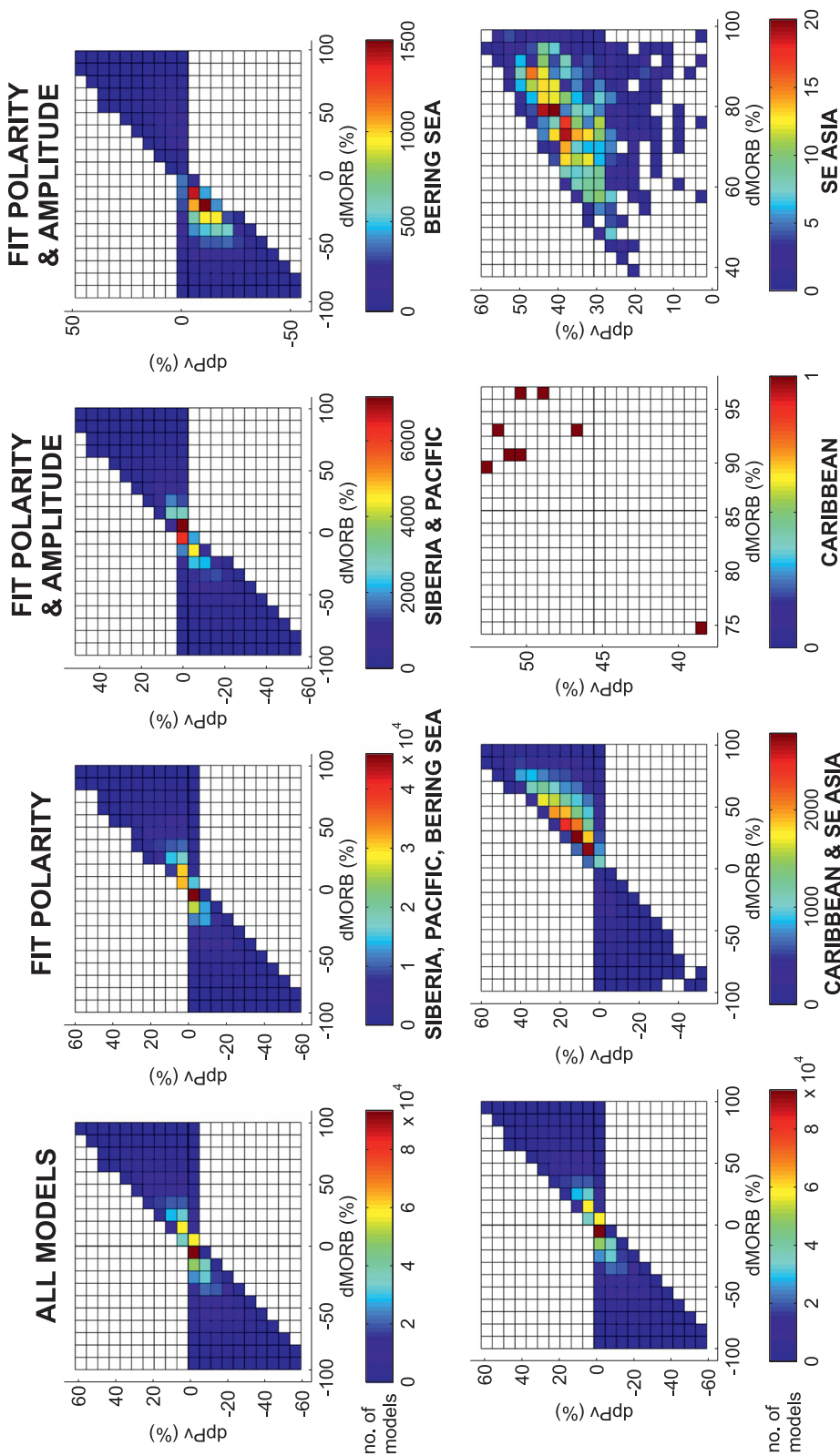


Figure A3. The result of modelling D'' reflections via a change in MORB content and concurrent change in temperature, where all the Mg, Fe and Al perovskite has converted to post-perovskite within the MORB (same simulation as in Fig. A2). Plotted above are 2-D frequency distributions showing number of models versus change in MORB content and change in post-perovskite content from above to below the D'' discontinuity. Left-hand column shows the distribution for 1 million initial models, other columns show the remaining models after fitting waveform polarities and amplitudes in different regions. Note that in this figure, dPv (per cent) is the change in volume percentage of pV over all the minerals present, as opposed to Figs 8 and 9 where it is the change in the percentage of pV within $(Pv + pV)$.

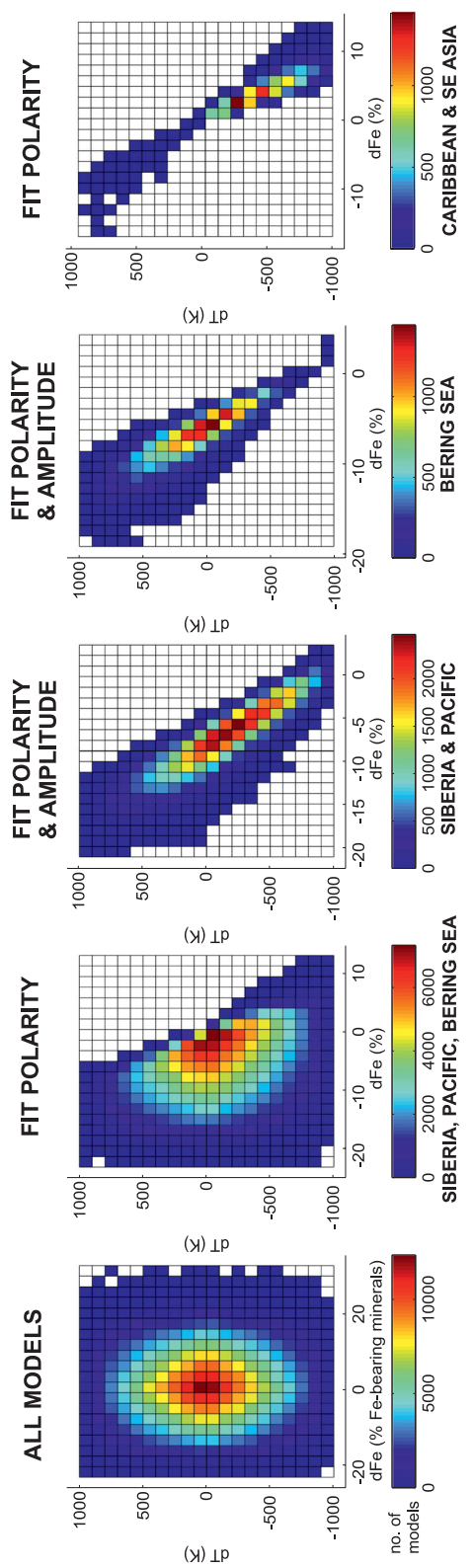


Figure A4. The result of modelling D'' reflections via a change in iron content and concurrent change in temperature across the discontinuity. We have plotted 2-D frequency distributions showing number of models versus change in iron content and change in temperature from above to below the D'' discontinuity. Left-hand plot shows the distribution for 1 million initial models, other plots show the remaining models after fitting waveform polarities and amplitudes in different regions. Change in iron content is expressed as volume percent change in Fe-bearing minerals, that is, FeSiO₃ and FeO. Note that no models fit both amplitudes and polarities in the Caribbean and Southeast Asia, that is, those regions with a negative PdP and positive SdS.

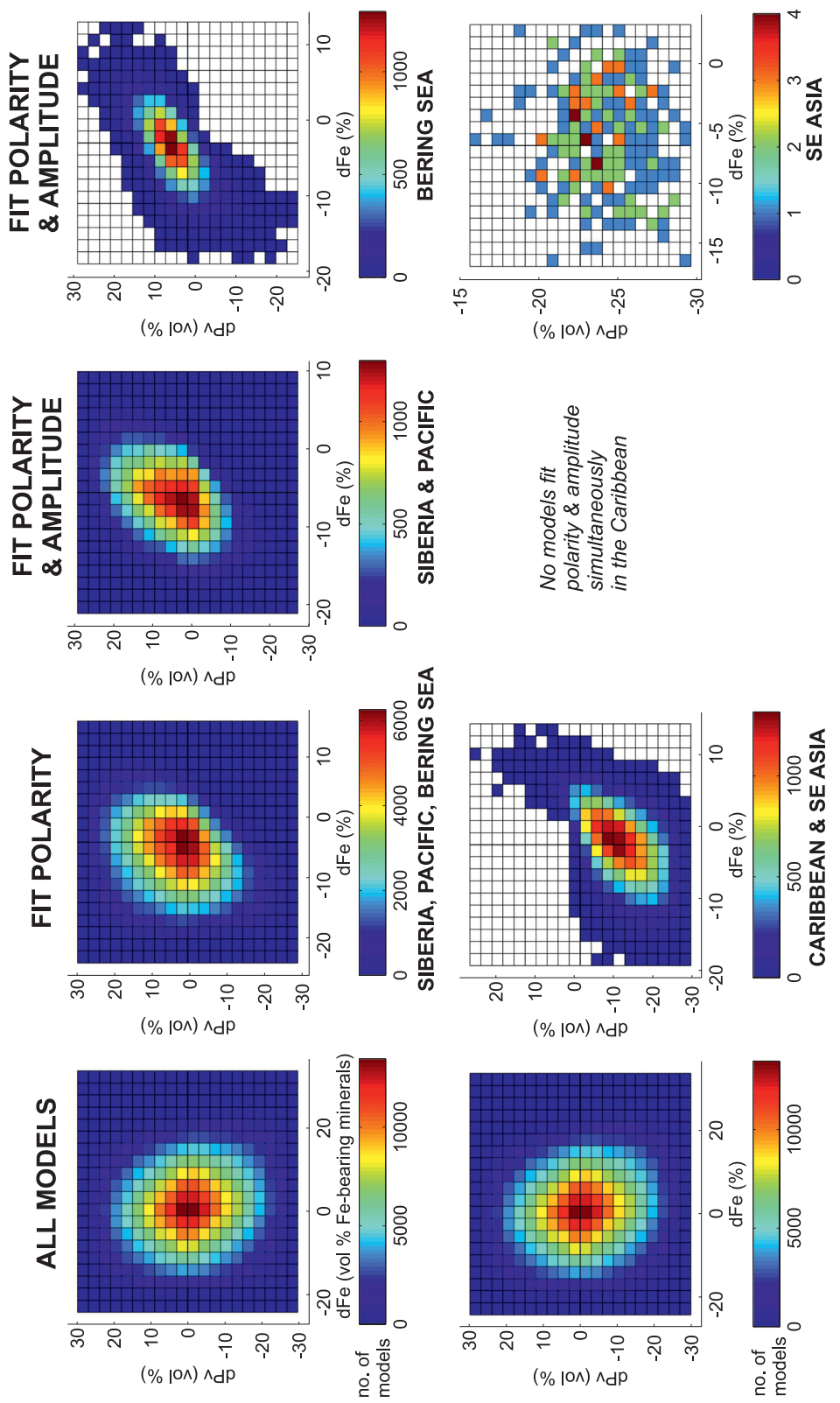


Figure A5. The result of modelling D'' reflections via a simultaneous change in iron content, change in perovskite content and change in temperature across the discontinuity. Shown in the figure are 2-D frequency distributions displaying number of models versus change in perovskite content from above to below the D'' discontinuity. Left-hand plot shows the distribution for 1 million initial models, other plots show the remaining models after tuning wavevector polarities and amplitudes in different regions. Change in iron content is expressed as volume percent change in Fe-bearing minerals, that is, FeSiO_3 and FeO . Change in perovskite content is expressed as volume percent change in $(\text{Mg}, \text{Fe})\text{SiO}_3$.

APPENDIX B

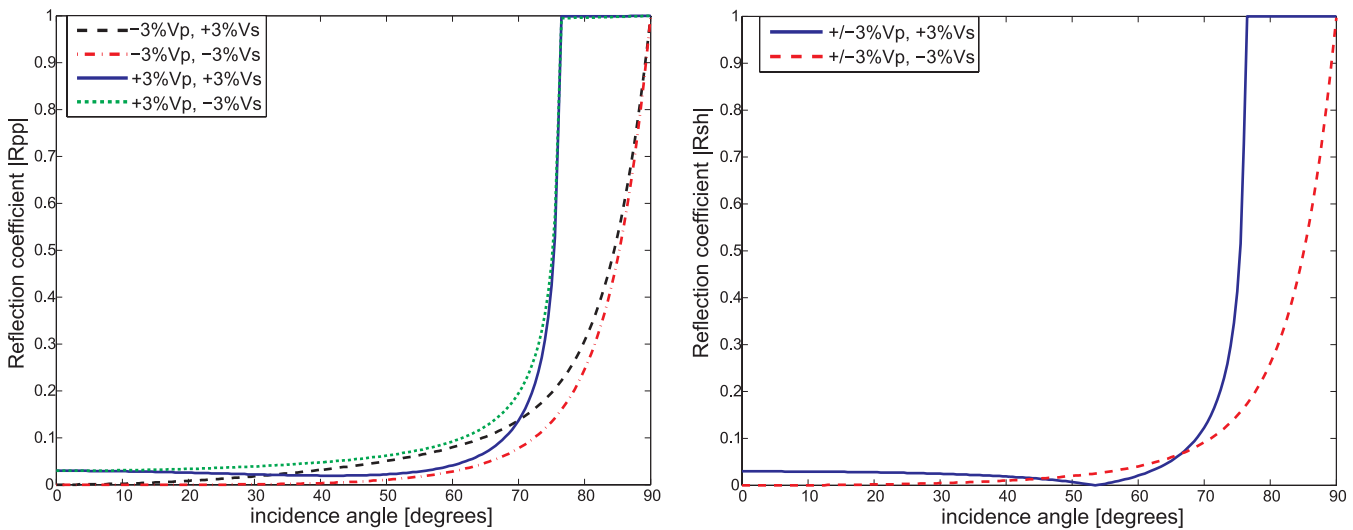


Figure B1. Magnitude of the reflection coefficient for P (left) and S (right) wave reflections at D'' as a function of take-off angle and for positive and negative changes in P and S velocity. Note that the P reflection coefficient depends on both the change in P -wave velocity and the change in S -wave velocity.